JACS
JOURNAL OF THE AMERICAN CHEMICAL SOCIETY
pubs.acs.org/JACS
Article

Dispersion and Steric E ects on Enantio /Diastereoselectivities in Synergistic Dual Transition Metal Catalysis

Bo Li Hui Xu Yanfeng Dang and K. N. Houk

Cite This: J. Am. Chem. Soc. 2022 144 1971 1985

ABSTRACT: Comprehensive computational studies were carried out to explore the mechanisms of enantioselective Cu/Pd and stereodivergent Cu/Ir dual-catalytic syntheses of , -disubstituted -amino acids (-AAs). A chiral copper azomethine ylide undergoes facile -allylation with racemic π-allylpalladium species or stereopure π-allyliridium complex to stereoconvergently or stereodivergently furnish single/double stereocenters, respectively. Stereoselectivity at the -center is controlled by the facial selectivity of -allylation with respect to the prochiral nucleophile. Despite apparently similar transition-state assemblies, computational models and distortion/interaction analyses disclose versatile modes of stereoinduction wherein the copper azomethine ylide species can face-selectively intercept metal π-allyl intermediates utilizing attractive dispersion interactions and/or sterically caused distortions. Generation of the β-stereocenter in the Cu/Ir system relies on a stereospeci cally generated allyliridium complex and electronically controlled branched-to-linear selectivity, while the dual Cu/Pd system yields a linear monochiral product due to steric factors and π π stacking interactions. The studies demonstrate on a molecular level how ligand-encoded chiral information is transferred to the -/β-sites of the resulting -AAs and how the mode of regio-/stereoselection is altered by differences in transition-metal-stabilized coupling partners. To facilitate studies of stereoselective catalysis, a suite of analytical tools to extract controlling factors for asymmetric induction is demonstrated.

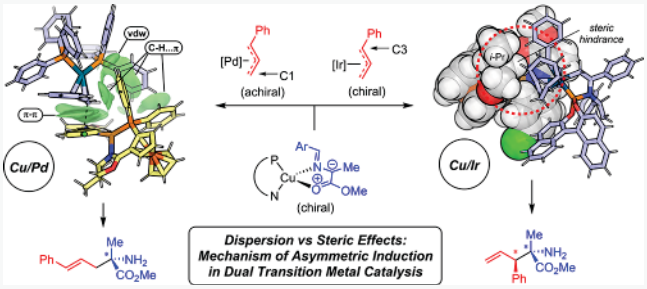

1. INTRODUCTION

The absolute and relative con gurations of chiral molecules with multiple stereogenic centers determine the functionalities of essential biomacromolecules such as proteins and nucleic acids as well as a wide spectrum of bioactive natural products and pharmaceuticals.[1] However, the one-step catalytic construction of multiple stereogenic centers with full control of enantio- and diastereoselectivities remains a synthetic challenge.[2] Since the seminal work of Carreira et al. in 2013,[3] the strategy of dual catalysis in which two chiral catalysts are exploited to exercise control over the corresponding stereocenters to stereodivergently access all permutations of product stereoselectivity has been intensely researched.[4] While earlier explorations focused more on merging transition-metal (TM) catalysis with organocatalysis,[3 11] the dual TM variant was not reported until the stereodivergent Zn/Ir dual-catalytic -allylation of -hydroxyketones by Zhang in 2016.[12] Subsequent years have witnessed the advancement and diversi cation of stereodivergent dual TM catalysis[4,13] by Zhang,[14 16] Wang,[17,18] Hartwig,[19] Zi,[20] and He.[21] Utilizing TM reactivities, these protocols provide stereodivergent access to multichiral molecules from identical starting materials,[4,13] providing an array of concise enantio-/diastereoselective methods with new opportunities toward diversity-oriented asymmetric synthesis and library design.[4]

While synergistic catalysis triggered much computational effort,[22 25] theoretical studies on stereodivergent dual TM catalysis remain limited.[24,25] Sunoj et al. recently investigated a related synergistic Cu/Ir system, highlighting the role of noncovalent interactions in absolute and relative stereocontrol.[24] Notwithstanding the expanding scope of reported reactions,[4,13 21] little is known about how differences in TM-stabilized chiral partners influence the mechanism and nature of stereorecognition. Recent studies of organometallic stereoinduction have established the role of dispersion interactions as the control element for reactions featuring large ligand architectures,[26 29] and new asymmetric systems have been developed by use of large substituents or heavy elements,[26] complementing the sterically driven design principle. Attractive dispersion interactions can be general in dual TM catalysis,[24,25] but due to the high expense of quantum mechanical computations (typically involving 150 250 atoms) and the difficulty for extracting meaningful information from overly

Received: December 2, 2021
Published: January 20, 2022

https://doi.org/10.1021/jacs.1c12664
J. Am. Chem. Soc. 2022 144 1971 1985

complicated transition structures, insight into the influence of dispersion effects on stereoselectivities of relevant systems and how they compare to steric repulsions are not usually obtained.

To explore the possible stereocontrolling dispersion and steric effects in such systems, we have performed quantum-mechanical studies on two dual TM-catalyzed syntheses of , -disubstituted -amino acids (-AAs) as shown in Scheme 1. In

Scheme 1. Representative Asymmetric Bimetallic Dual-Catalytic Syntheses of Non-Proteinogenic -Amino Acids Studied in the Present Work[15 17 30]

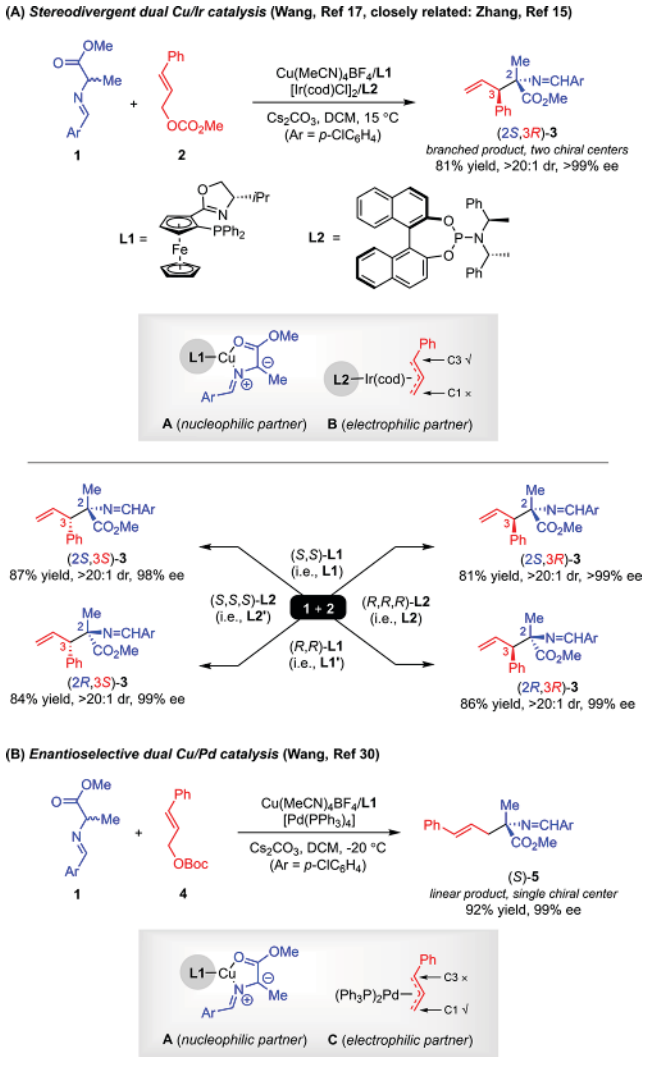

2018, Wang[17] and Zhang[15] independently reported two closely related, fully stereodivergent Cu/Ir systems to synthesize - AAs bearing vicinal quaternary/tertiary ,β-stereocenters. The reaction reported by the Wang group (Scheme 1A) is investigated here in parallel with their early work on a similar enantioselective Cu/Pd system (Scheme 1B).[30 32] The two reactions employ the identical prochiral nucleophile, i.e., copper azomethine ylide species, a key chiral synthon whose utility has been actively studied in recent years especially in the context of dual TM catalysis.[15 18,20,31,33,34] These two systems are excellent for studying the stereorecognition of the representative prochiral nucleophile **A** with meta-π-allyl species **B** (chiral) or **C** (achiral). We have explored in greater depth the origins of stereoselectivity in these cases, given the ubiquity of metal-enolate-type prochiral nucleophiles. We describe a suite of analytical tools that differentiates the stereocontrolling factors in dual-catalytic transformations.

2. COMPUTATIONAL METHODS

Density functional theory (DFT) calculations were carried out mostly in the Gaussian 09 package.[35] We used the M06-L functional throughout due to its good performance for transition-metal chemistry and noncovalent interactions as well as the relatively low computational cost as a local functional.[36] Geometry optimizations and vibrational frequency calculations were conducted with a mixed basis set that combines the Stuttgart Dresden SDD effective core potential (ECP) basis set[37] for transition metals (Fe, Cu, Pd, Ir) with 6-31G(d) for all other elements. Single-point energies were subsequently calculated using the def2-TZVP basis set[38] and the Truhlar-Cramer universal solvation model based on density (SMD) for CH_2Cl_2.[39] All thermodynamic quantities (concentration 1 mol/L, temperature 253.15 K for the Cu/Pd system,[30] 288.15 K for the Cu/Ir system[17]) were evaluated in the GoodVibes code[40] with quasi-rigid-rotor-harmonic-oscillator approximations (frequency cutoff 100 cm^{-1}).[41] Absolutely localized molecular orbital energy decomposition analysis (ALMO-EDA)[42] implemented in the Q-Chem software package[43] was performed with M06-L/def2-TZVP. Multiwfn[44] was utilized to produce steric contours,[45] compute buried surface areas,[46] and van der Waals potentials[47] and to analyze noncovalent interactions with the independent gradient model (IGM).[48] Molecular visualizations were carried out in CYLview and PyMOL.[49]

3. RESULTS AND DISCUSSION

3.1. Mechanism of Synergistic Cu/Pd Catalysis. The stereorecognition of Pd^{II}/Ir^{III}-π-allyl species by Cu^{I}-azomethine ylide is the basis of stereocontrol in dual-catalytic stereodivergent -AA syntheses.[15,17,30] Molecular-level information about the formation and subsequent reactions of these species is achieved in this report. To understand the origin of -center stereoselectivity, we rst studied the Cu/Pd system in Scheme 1B with the (*S*,*S*)-**L1** ligand (designated as **L1**).

Formation of N-Copper Azomethine Ylide and Allylpalladium Species. We begin by investigating the formations of the prochiral nucleophile and the allylpalladium electrophile. As shown in Figure 1A, the copper azomethine ylide has two

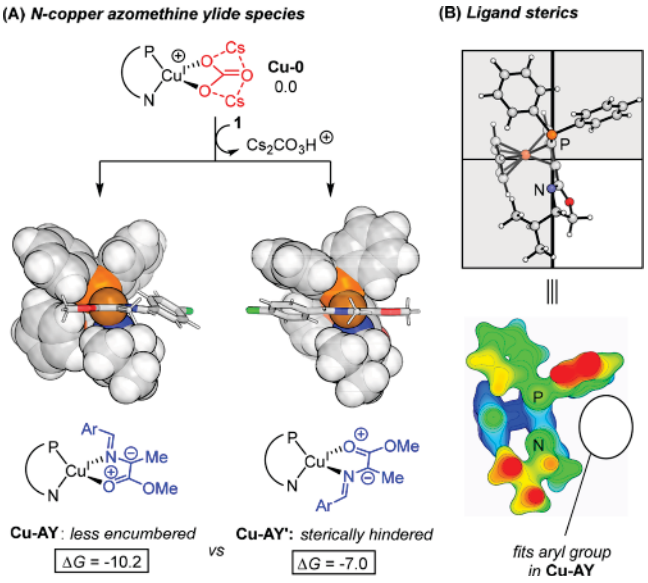

Figure 1. Copper azomethine ylide species. (A) Formation and stereoisomers. (B) Ligand steric environment.

https://doi.org/10.1021/jacs.1c12664
J. Am. Chem. Soc. 2022 144 1971 1985

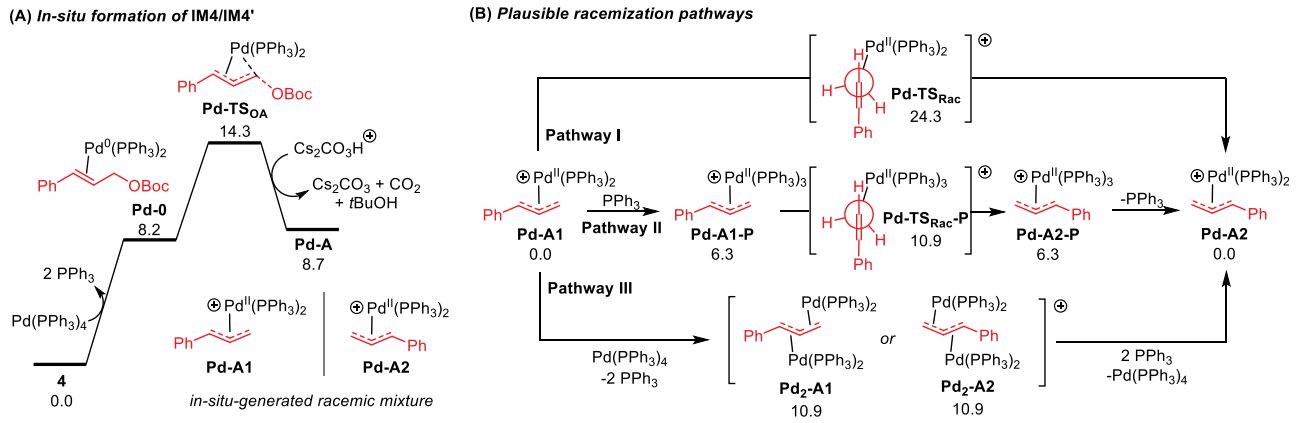

Figure 2. (A) Free energy pro le for the in situ formation of allylpalladium. (B) Stereochemical stability analysis by free energy pro les of possible racemization pathways.

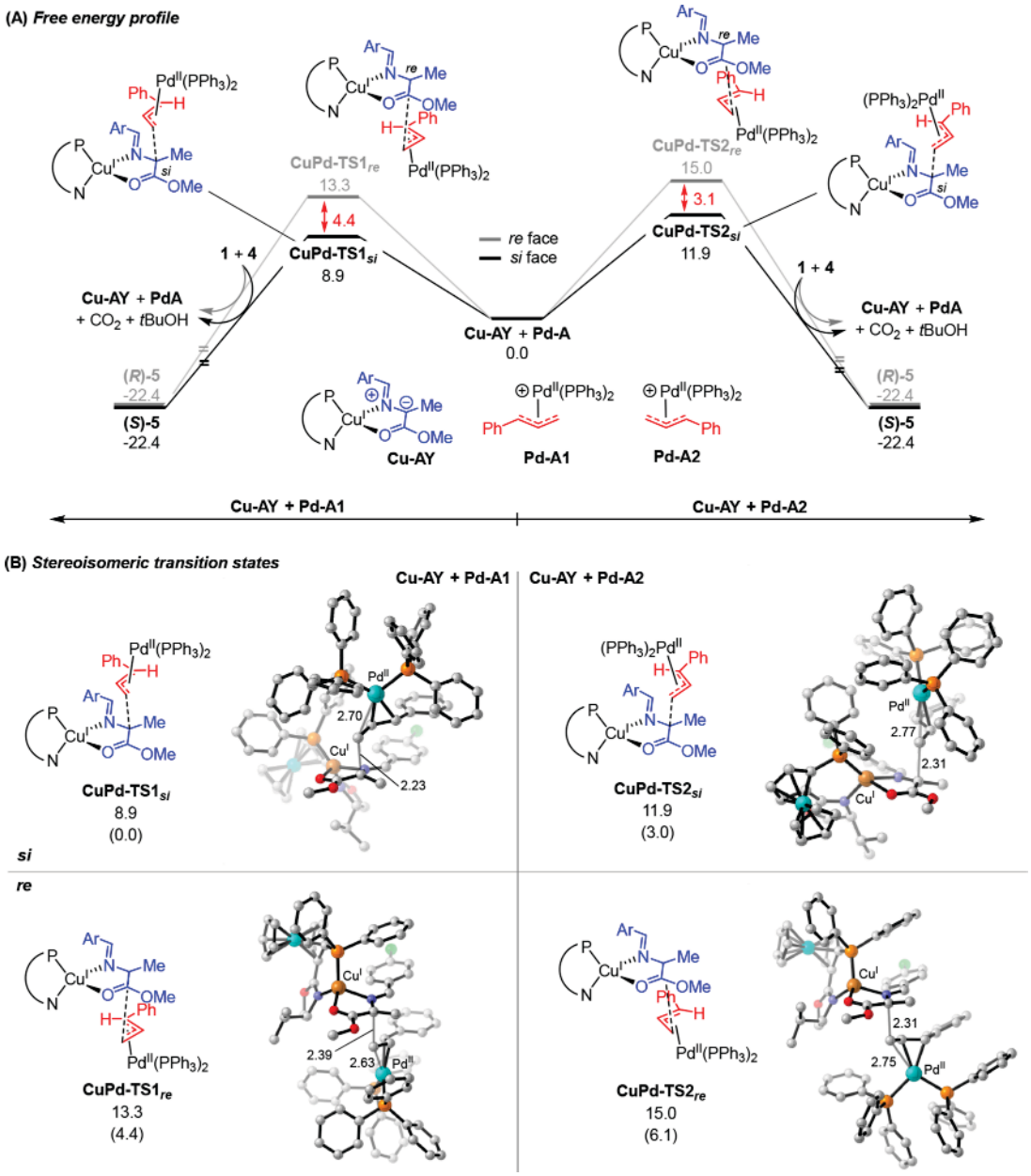

Figure 3. (A) Free energy pro le and (B) stereoisomeric transition states for the -allylation of Cu^{I} azomethine ylide by Pd^{II}-allyl species.

https://doi.org/10.1021/jacs.1c12664
J. Am. Chem. Soc. 2022 144 1971 1985

possible stereoisomers **Cu-AY** and **Cu-AY** . Formation of the former is more exergonic by a substantial 3.2 kcal/mol due to a favorable ligand-substrate arrangement where the bulky *p*-C_6H_4Cl aryl group is on the less encumbered side of **L1** (Figure 1B). Hence, **Cu-AY** is likely to be the main form of the copper azomethine ylide[25,50] and is focused on in subsequent computations.

The allylpalladium is formed by the mechanism shown in Figure 2A. The initial Pd^0 catalyst undergoes ligand exchange with **4** to form an η^2-complex **Pd-0** (8.2 kcal/mol), and the allylic C O bond is cleaved by oxidative addition (**Pd-TS$_{OA}$** 14.3 kcal/mol), leading to the Pd^{II}-π-allyl complex **Pd-A** (8.7 kcal/mol, note that **A** denotes allyl group in all notations) as a racemic mixture (we denote the two enantiomers by **Pd-A1** and **Pd-A2**). This is to be contrasted with the Cu/Ir dual-catalytic system where the chiral ligand **L2** renders the Ir^{III} π-allyl complex stereopure.

To evaluate whether the enantiomers of **Pd-A** could interconvert within the time scale of the reaction, the free energy pro les of three representative mechanisms were computed (Figure 2B).[51] In pathway **I**, **Pd-A1** undertakes η^3 η^1 η^3 (i.e., π σ π) isomerization toward **Pd-A2**,[52] which requires a high 24.3 kcal/mol barrier (via **Pd-TS$_{Rac}$**). Ligation of an extra PPh_3 to Pd^{II} can stabilize the transition state and promote the η^3 η^1 η^3 isomerization, giving rise to pathway **II** whose barrier is considerably lowered (10.9 kcal/mol via **Pd-TS$_{Rac}$-P**).[53] We also examined the nucleophilic displacement mechanism (pathway **III**)[54] in which a second $[Pd(PPh_3)_2]$ motif substitutes the original one in **Pd-A1** from the opposite face of allyl to yield **Pd-A2**. Pathway **III** involves bipalladium-π-allyl intermediates **Pd$_2$-A1** and **Pd$_2$-A2** whose stabilities are similar to **TS3**. Hence, the racemization needs to overcome 10.9 kcal/mol via pathways **II** or **III**. This is comparable to the barriers of the following bond formation (9 12 kcal/mol, discussed later).

According to these results, **Pd-A1**/**Pd-A2** may be unable to experience substantial interconversions as the reaction proceeds.[55] Ideal stereocontrol would require that **Cu-AY** stereoselectively consume both enantiomers of **Pd-A**. As the stereoselectivity is determined by the face from which the prochiral -C of **Cu-AY** is approached by **Pd-A**, it is likely that **Cu-AY** has a facial preference that is independent of the absolute con guration of the Pd^{II} π-allyl, thus achieving stereoconvergence toward a single product stereoisomer. The proposed mechanism is explored in the next section.

Mechanism of Stereoselective -Allylation. We studied the -allylation of **Cu-AY** with the **Pd-A** racemate.[56] For the two enantiomers of **Pd-A**, the two possible approaches (*re* and *si*) to **Cu-AY** result in a total of four stereoisomeric C C bond-forming TSs (Figure 3). The lower energy TSs **CuPd-TS1$_{si}$** (8.9 kcal/mol, with **Pd-A1**) and **CuPd-TS2$_{si}$** (11.9 kcal/mol, with **Pd-A2**) lead to the same enantiomer (*S*)-**5**, the main product of this system.[17] The favorability of the *si*-TS over the *re*-TS is 4.4 and 3.1 kcal/mol, respectively, both implying high stereoselectivity.

Origin of Enantioselectivity. Since the *si*-face approach of **Cu-AY** is favored regardless of the absolute con guration of **Pd-A**, it is critical to understand how the stereochemical elements of **Cu-AY** result in such a strong facial preference. The facial discrimination of metal-enolate-type prochiral nucleophiles comprises a rather general problem in stereo-divergent dual catalysis,[12 21] and the very frequently employed *N*-metalated azomethine ylide is regarded here as a representative system.[15 18,20,31,33,34] The asymmetric environment of **Cu-AY** is analyzed in Scheme 2. The preferred

Scheme 2. Analysis of the Origin of -Stereoselectivity

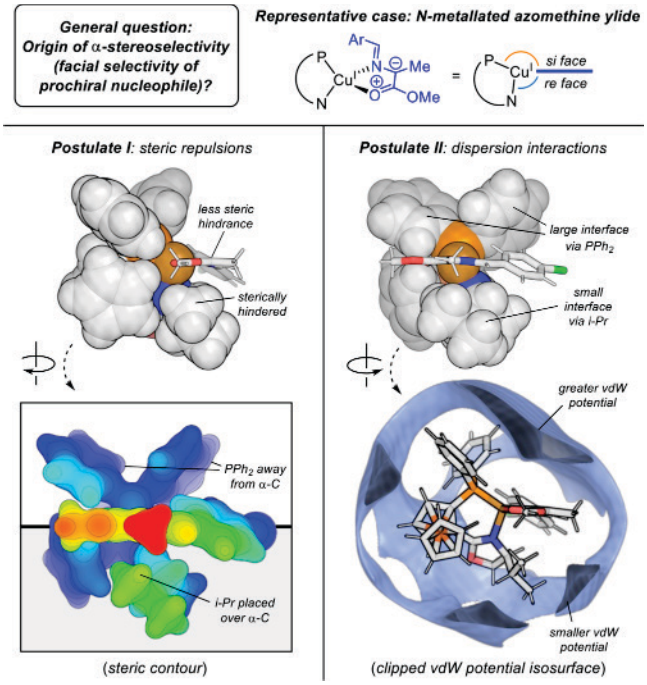

[a]Various renditions of **Cu-AY** are shown. The observed *si* attack is from the top, *re* attack from the bottom.

direction of attack by **Pd-A** could originate from steric hindrance[57,58] and/or dispersion interactions.[26 29] On the one hand, the biased sterics on the two faces (left sub gures in Scheme 2) might cause larger distortions and steric repulsions when -allylation occurs at the more encumbered *re* face over which a *i*-Pr group on the oxazoline unit of **L1** could hinder the approach of allyl-metal species (postulate **I**). On the other hand, since the phosphino motif of **L1** over the *si* face could potentially provide large π-interfaces[59] with a greater surface area than the 4-isopropyl-oxazoline unit over the *re* face, dispersion interactions might favor *si* attack (postulate **II**, right sub gures). This is illustrated by an evaluation of van der Waals (vdW) potential, which calculates the potential energy of a He atom interacting with the molecule of interest to probe sites with attractive vdW interactions.[47] The analysis discloses a greater distribution of negative (attractive) values on the *si* face.

To disentangle the possible controlling factors, distortion/interaction (D/I) analysis[60,61] was performed for the four stereoisomeric TSs to quantitate (a) the interaction strength between **Cu-AY** and **Pd-A** as they reach each TS and (b) the associated structural distortions in each reactant. According to Figure 4A, the barrier differences originate primarily from the much greater interaction energies in **CuPd-TS1$_{si}$** (29.6 kcal/mol) and **CuPd-TS2$_{si}$** (26.7 kcal/mol) than **CuPd-TS1$_{re}$** (19.1 kcal/mol) and **CuPd-TS2$_{re}$** (18.8 kcal/mol), which is compatible with postulate **II**.

We further explored postulate **II** by a visual analysis of noncovalent interactions (NCIs).[62] We adopted the independent gradient model (IGM) due to its capability for extracting intermolecular NCIs. These are shown by the isosurface of

https://doi.org/10.1021/jacs.1c12664
J. Am. Chem. Soc. 2022 144 1971 1985

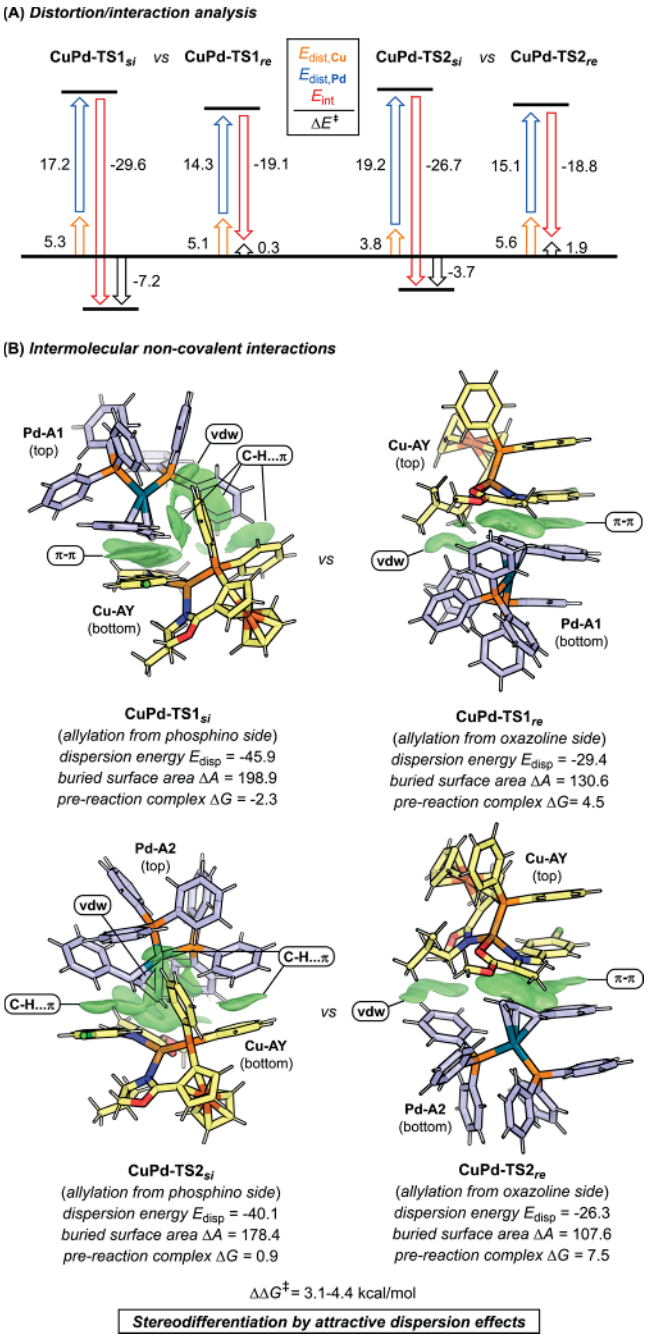

Figure 4. Origin of enantioselectivity in Cu/Pd synergistic catalysis. (A) Distortion/interaction analysis. (B) Visualization of intermolecular noncovalent interactions. Dispersion energies from EDA, buried surface areas (Å^2), and free energies of prereaction complexes are provided alongside.

δg^{inter} function (green blobs in Figure 4B).[48] In comparing **CuPd-TS1**$_{si}$ with **CuPd-TS1**$_{re}$, a signi cant difference in **L1**···**Pd-A1** nonbonding interactions is observed. The phosphino unit of **L1** in **Cu-AY** can interact with **Pd-A1** with a variety of C H···π/vdW interactions in **CuPd-TS1**$_{si}$ (buried surface area 198.9 Å^2), while **CuPd-TS1**$_{re}$ (buried surface area 130.6 Å^2) only allows **Pd-A1** to interact with a relatively small *i*-Pr group on the oxazoline unit of **L1**. The same analyses also revealed larger vdW contact in **CuPd-TS2**$_{si}$ than in **CuPd-TS2**$_{re}$ (Figure 4B). The importance of these interactions is supported by energy decomposition analysis (EDA), which discloses considerably stronger dispersion interactions in the *si*-TSs (ca. 13 17 kcal/mol). Moreover, there are shallow PES minima before the TSs, and these prereaction complexes (PRCs) have energy differences related to the corresponding TSs but are free of the transition-state bonding interactions, thus providing an additional estimate for the nonbonding effects. As anticipated, the *si*-PRCs are 6.8 (for **CuPd-TS1**) and 6.6 kcal/mol (for **CuPd-TS2**) more stable than the *re*-PRCs, which correlate with the relative barriers of the TSs. These differences are due to more stabilizing dispersion in the *si* approach.

In summary, the above-presented multimodal stereochemical analyses, including distortion/interaction analysis, noncovalent interaction plots, buried surface areas, dispersion energies, and relative stabilities of pre-reaction complexes, consistently point to attractive dispersion effects as the origin of enantioselectivity (i.e., the *si* facial preference of prochiral nucleophile) for the present Cu/Pd system.

Origin of Regioselectivity. Regiocontrol is fundamental for selective allylic substitutions.[51,63 68] Here, the regiochemistry for the attack of metal-allyl species determines the number of stereocenters. As depicted in Scheme 3, the Cu/Pd dual

Scheme 3. Regiochemistry Comparison for the Reactions Investigated in the Present Work

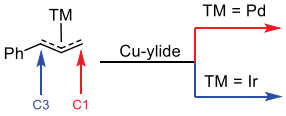

	product connectivity	number and source(s) of chiral center(s)
TM = Pd	*linear*	***one stereocenter*** (α-C of azomethine ylide)
TM = Ir	*branched*	***two stereocenters*** (α-C of azomethine ylide, C3 of allyl complex)

catalysis affords linear product **5** with one -stereocenter.[30] This differs from the synergistic Cu/Ir system, which furnishes branched product **3** with successive ,*β*-stereocenters.[17] We next explore the regioselectivity of the Cu/Pd system, and the Cu/Ir catalysis will be discussed later.

Figure 5A analyzes the two -allylation TSs for branched products. The barriers of branched TSs **CuPd-TS1** $_{si}$ (**Cu-AY** with **Pd-A1**) and **CuPd-TS2** $_{si}$ (**Cu-AY** with **Pd-A2**) are higher than the linear TSs **CuPd-TS1**$_{si}$ and **CuPd-TS2**$_{si}$ by 1.6 and 1.7 kcal/mol, respectively, which explains the linear selectivity. Notably, the linear-to-branched selectivity is independent of the absolute con guration of **Pd-A**, and both enantiomers of **Pd-A** prefer the unsubstituted terminus.

Distortion/interaction analysis shows that both branched TSs have higher distortion energies than the linear TSs, while the interaction energies are not large enough to compensate for the unfavored distortions. The regioselectivity originates from at least two effects. First, an inspection of the steric environment of **Pd-A** shows that C3 is sterically hindered (Figure 5B). To expose C3 to the nucleophilic partner, the breaking Pd C bond in branched TSs (Pd C3 3.08 Å for **CuPd-TS1** $_{si}$, 3.01 Å for **CuPd-TS2** $_{si}$) has to be more stretched than those in linear TSs (Pd C1 2.70 Å for **CuPd-TS1**$_{si}$, 2.77 Å for **CuPd-TS2**$_{si}$), which explains the distortion energies. Second, attacks at the C1 site create a suitable geometrical relationship for NCIs between the Ph group of **Pd-A** and the *p*-C_6H_4Cl group of **Cu-AY** (π π in **TS4a**, C H···π in **TS5a**, see Figures 5C and 4B, respectively), but the same groups are too distant in the branched TSs to afford such stabilizations. Hence, the regioselectivity in the Cu/Pd system

https://doi.org/10.1021/jacs.1c12664
J. Am. Chem. Soc. 2022 144 1971 1985

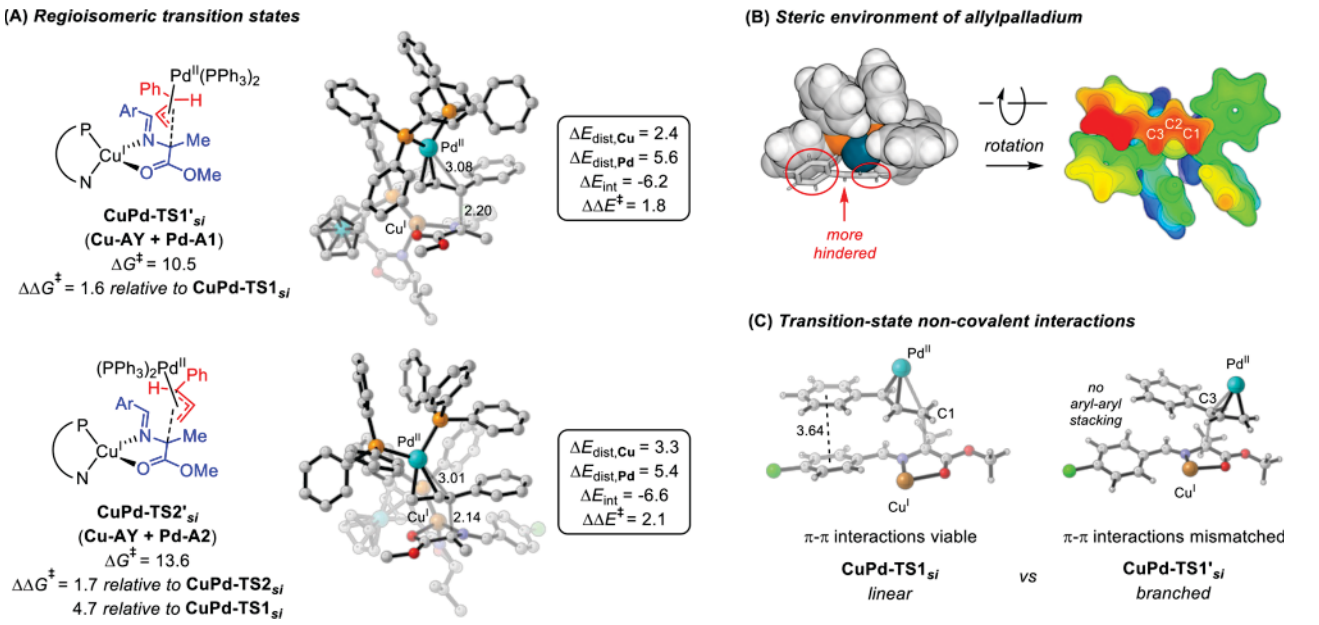

Figure 5. Origin of regioselectivity in synergistic Cu/Pd system. (A) Regioisomeric transition states providing branched products with free energy barriers and D/I energies. (B) Steric environment of π-allylpalladium species. (C) Comparison of key NCI in regioisomeric TSs; ligands omitted for clarity.

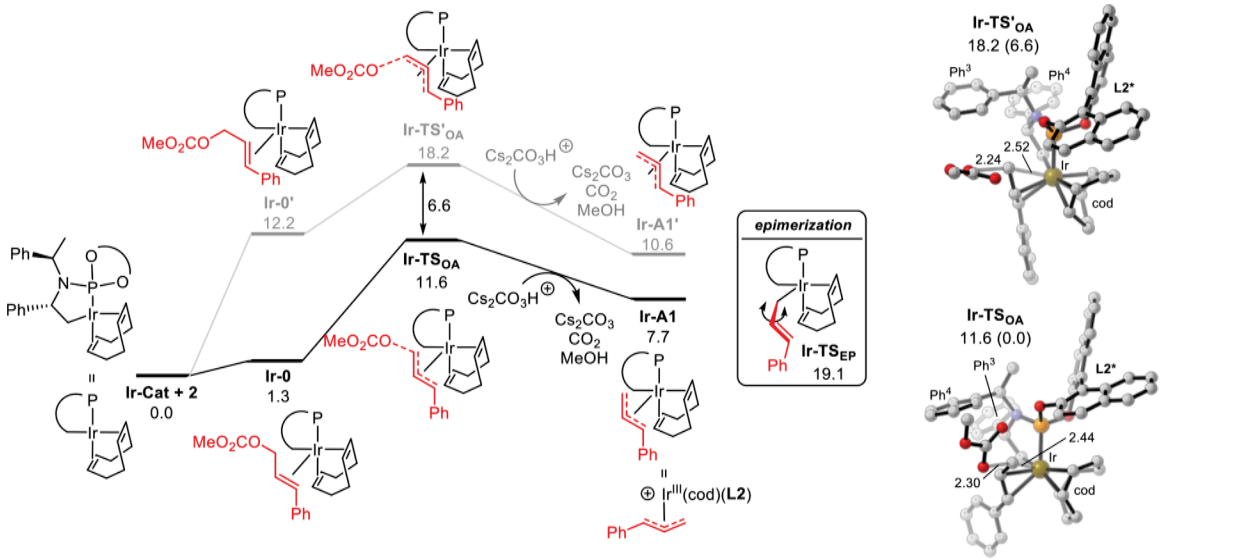

Figure 6. Formation and epimerization of allyliridium interemediate. For simplicity, **L2** is also used to denote the phosphoramidite ligand adopting the metallacyclic mode of coordination.

is likely to be a consequence of steric repulsions and dispersion effects.

3.2. Mechanism of Synergistic Cu/Ir Catalysis. For the second half of the present study, we explore the mechanism whereby the coupling between two chiral partners, the copper azomethine ylide and the π-allyliridium complex, gives rise to two consecutive ,β-stereogenic centers in the selected Cu/Ir dual-catalytic system (Scheme 1A).[17] We assume for now that **L1** and (*R*,*R*,*R*)-**L2** (denoted simply by **L2**) are used, and we will later discuss the other combination of **L1** with (*S*,*S*,*S*)-**L2** (**L2**) to shed light on the origin of stereodivergence.[17] For ease of understanding, we avoid discussing (*R*,*R*)-**L1** (i.e., **L1**) throughout, as the results will be equivalent. We skip discussions on the prochiral nucleophile because the same Cu-azomethine ylide species **Cu-AY** is involved.

Formation of Allyliridium Species. The selected Cu/Ir dual-catalytic -AA synthesis is empowered by an Ir-based asymmetric allylic substitution system[69,70] using phosphoramidite ligand **L2**,[71] which involves an activated catalyst **Ir-Cat** with a metallacyclic structure.[72] The catalysis commences with the generation of Ir^{III}-allyl species **Ir-A** from **Ir-Cat** (Figure 6).[69,72 75] The entrance of cinnamyl methyl carbonate substrate **2** into the coordination sphere results in an η^2-complex **Ir-0**, which affords allyliridium species **Ir-A1** via oxidative addition (**Ir-TS$_{OA}$**). The stereoisomeric pathways are computed to be at least 6.6 kcal/mol less favored (more details are provided in the SI). The predicted **Ir-A1** is supported by the X-ray structure of related phosphoramidite ligand-derived allyliridium.[74] Similar to the Cu/Pd system, a high epimerization barrier (11.4 kcal/mol, at least 1.5 kcal/mol

https://doi.org/10.1021/jacs.1c12664
J. Am. Chem. Soc. 2022 144 1971 1985

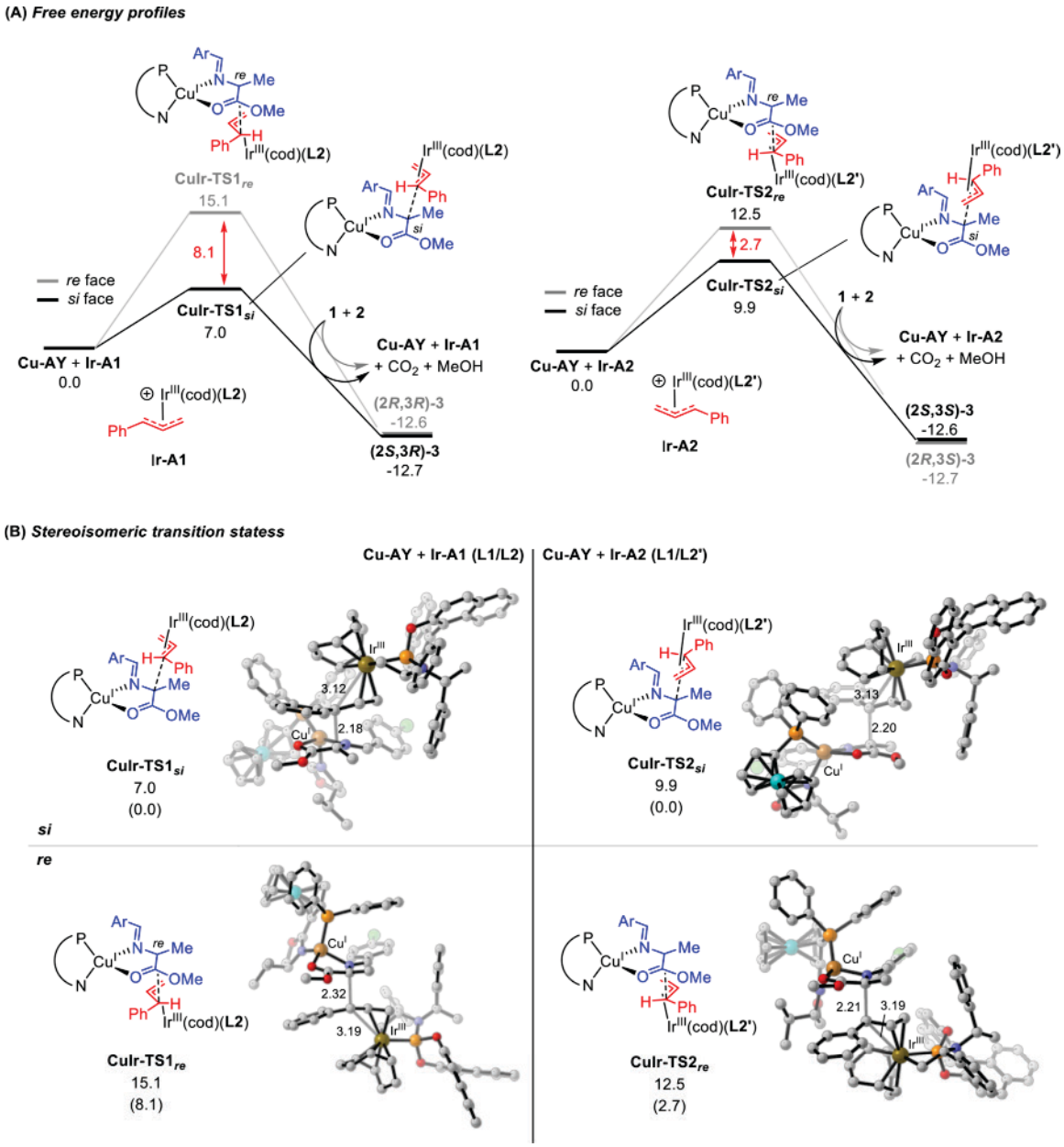

Figure 7. Mechanism of stereodivergent -allylation in the dual Cu/Ir system. (A) Free energy pro les and (B) stereoisomeric transition states for the -allylation of chiral Cu^{I}-azomethine ylide species by chiral Ir^{III}-allyl species.

higher than bond formation) suggests that the stereochemical structure of **Ir-A1** should be largely static.

We note that the absolute con guration of allyliridium translates into the β-center diastereoselectivity of the reaction because outer-sphere bond formation proceeds via a stereo-de ned *anti*-displacement. An analysis for the mode of β-site stereoselection is provided in the Supporting Information.

Mechanism of Stereodivergent -Allylation. The stereo-divergent -allylation of copper azomethine ylide **Cu-AY** with allyliridium **Ir-A1** (when using **L2**) or the enantiomer **Ir-A2** (when using **L2**) is investigated. The facial preference of **Cu-AY** determines the absolute con guration of the -stereo-center. Figure 7 presents the free energy pro le for the stereodivergent -allylation between **Cu-AY** and **Ir-A**. The copper azomethine ylide **Cu-AY** can consume either **Ir-A1** or **Ir-A2** with low barriers (<10 kcal/mol), which indicates high reactivity. Consistent with the Cu/Pd system, the *si* diastereo-face of **Cu-AY** is more favorable, the barrier differences being 8.1 kcal/mol (**CuIr-TS1**$_{si}$ vs **CuIr-TS1**$_{re}$) and 2.7 kcal/mol (**CuIr-TS2**$_{si}$ vs **CuIr-TS2**$_{re}$). We predict accordingly that (2*S*,3*R*)-**3** and (2*S*,2*S*)-**3** are generated, respectively, in the two cases, which agrees with experiments.[17]

Origin of Diastereoselectivity -Stereocenter). With the transition-state models established, we studied the facial discrimination for **Cu-AY** to gain insights into the -center diastereoselectivity (i.e., for the formation of 2*S* center when **L1** is employed). We begin with a distortion/interaction analysis (Figure 8). Although the *si* face of **Cu-AY** is consistently more favorable, the distortion/interaction energies suggest a mode of stereoselection distinct from the Cu/Pd system, with distortions playing a more important role. This is especially the case for **L1**/**L2** (i.e., **Cu-AY** and **Ir-A2**): While the distortion favors **CuIr-TS2**$_{si}$ by 3.9 kcal/mol, the interaction energies are almost identical. For **L1**/**L2** (i.e.,

https://doi.org/10.1021/jacs.1c12664
J. Am. Chem. Soc. 2022 144 1971 1985

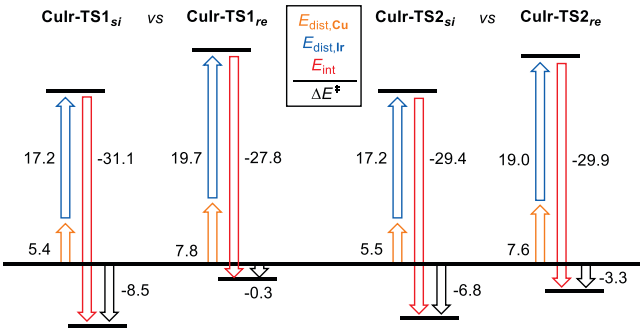

Figure 8. Origin of -center diastereoselectivity in the Cu/Ir dual-catalytic system from distortion/interaction analysis.

Cu-AY and **Ir-A1**), distortion and interaction energies contribute to the barrier difference by 4.9 and 3.3 kcal/mol, respectively, which also involves signi cant distortion-driven differentiation.

Recalling the analysis in Scheme 2, we speculate that versatile modes of asymmetric induction for the prochiral nucheophile **Cu-AY** are possible by simply changing the electrophilic coupling partner. Notably, the stereocontrol in dual catalysis is often assumed to be local in order to realize stereodivergence.[3] The connection between such interpretation and the underlying mode of stereoselection is not fully understood largely because of the difficulty of identifying the key stereocontrol elements from these involved bond-forming TSs. In what follows, we utilize the suite of visual analysis and energetic/physical-organic indices to unveil the nature of diastereofacial selection for the prochiral nucleophile.

First, we considered the distortion-controlled coupling of **Cu-AY** with **Ir-A2** (i.e., **L1**/**L2** , see Figure 9). According to D/I analysis and following our analysis in Scheme 2, we propose that the *si* diastereofacial preference originates from steric effects (i.e., postulate **I** holds). In fact, inspection of TSs reveals that the lower energy **CuIr-TS2**$_{si}$ complements the cod in **Ir-A2** with the phosphino unit of **L1**, while the higher energy **CuIr-TS2**$_{re}$ entails repulsions between cod and the 4-isopropyloxazoline unit of **L1** (see the bottom sub gures). The repulsions are reflected by the above-presented distortion energies and the greater Pauli repulsions in the disfavored **CuIr-TS2**$_{re}$ (110.0 kcal/mol) than in **CuIr-TS2**$_{si}$ (106.7 kcal/mol, see Table S2 for full EDA and Figure S5 for repulsive distances). On the other hand, contrary to postulate **II** (i.e., facial diastereoselection by dispersion), the favored **CuIr-TS2**$_{si}$ (buried surface area 161.7 Å^2) exhibits smaller dispersion energy (40.7 kcal/mol) than the disfavored **CuIr-TS2**$_{re}$ (44.1 kcal/mol, buried surface area 188.2 Å^2), and an assessment of the noncovalently bound prereaction complexes also suggests that **CuIr-RC2**$_{si}$ and **CuIr-RC2**$_{re}$ are equally stable. Inspection of the sphere(**Cu-AY**)/stick(**Ir-A2**) models in Figure 9 shows that the available molecular surface over the *si* face is not fully harnessed by **CuIr-TS2**$_{si}$, which explains the lack of *si*-favoring attractive dispersions. According to these results, we conclude that steric effects control the diastereo-face-selective -allylation of **Cu-AY** by **Ir-A2**.

We then explored the origin of diastereoselectivity for **L1**/**L2** (i.e., **Cu-AY**/**Ir-A1**) by again examining the posultates **I** and **II** (Figure 10). For postulate **I** (steric effects), **CuIr-TS1**$_{si}$ manifests a less encumbered arrangement by placing the allyl over the π-system of azomethine ylide, while **CuIr-TS1**$_{re}$ is destabilized by the steric repulsions over cod/4-isopropyl-

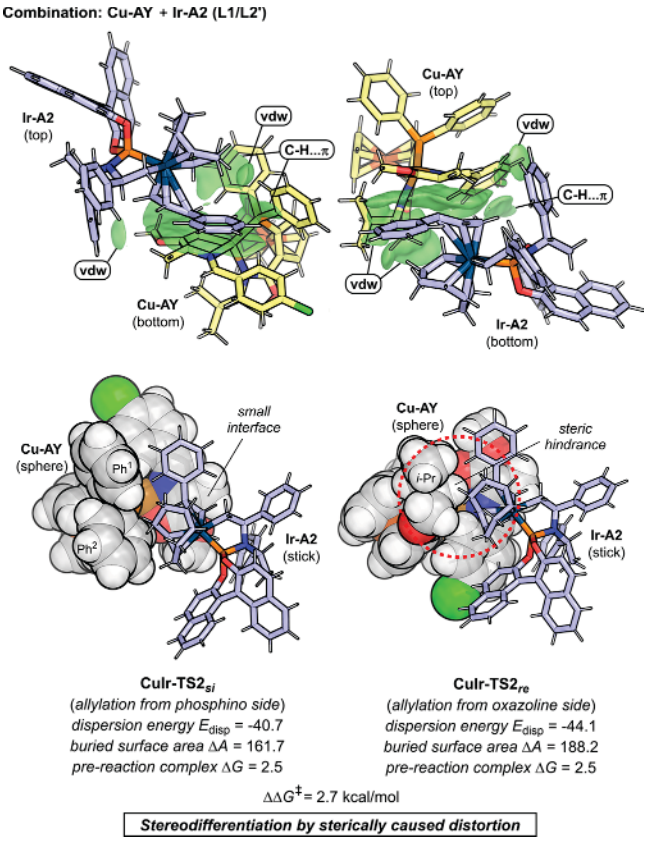

Figure 9. Origin of -center diastereoselectivity in the Cu/Ir system: **CuIr-TS2**$_{si}$ vs **CuIr-TS2**$_{re}$. Top: Intermolecular NCIs. Bottom: TSs shown in sphere(copper azomethine ylide)-stick(allyliridium) representation. Dispersion interaction energies, buried surface areas (Å^2), and free energies of PRCs are provided alongside.

oxazoline and -Ph^3/*p*-C$_6$H$_4$Cl interfaces; this is mirrored by the distortion energies (**CuIr-TS1**$_{re}$ 26.6 kcal/mol > **CuIr-TS1**$_{si}$ 22.7 kcal/mol) and repulsive distances (Figure S5). For postulate **II** (attractive dispersions), we observe greater dispersion energy (**CuIr-TS1**$_{si}$ 54.9 kcal/mol, **CuIr-TS1**$_{re}$ 45.2 kcal/mol), larger buried surface area (**CuIr-TS1**$_{si}$ 206.2 Å^2, **CuIr-TS1**$_{re}$ 168.7 Å^2), and higher stability of PRC (**CuIr-RC1**$_{si}$ 0.2 kcal/mol, **CuIr-RC1**$_{re}$ 11.9 kcal/mol) for the *si* face approach. Overall, the diastereofacial differentiation with **L1**/**L2** is dictated by the combined effects of sterically caused distortions and attractive dispersions.

The ndings to this point are indicative that, despite an identical prochiral nucleophile, similar metal allyl electrophiles and consistent modes of attack, the seemingly analogous TSs in Figures 3B and 7B involve different mechanisms of stereoselection that are based on dispersion and/or steric effects between the two coupling partners. How the asymmetric induction mechanism would change in more general situations of stereodivergent cooperative catalysis is yet to be investigated. To this end, the above-presented energetic and physical organic parameters are expected to be useful tools for extracting relevant information about stereoselection, thus providing more rigorous insights for the proper interpretation of these extended and involved computational models.

Origin of Regioselectivity. Contrasting the formation of linear product in the previous Cu/Pd system, the synergistic Cu/Ir catalysis affords branched products with successive „β-stereocenters (Scheme 3). The regioisomeric TSs for the

https://doi.org/10.1021/jacs.1c12664
J. Am. Chem. Soc. 2022 144 1971 1985

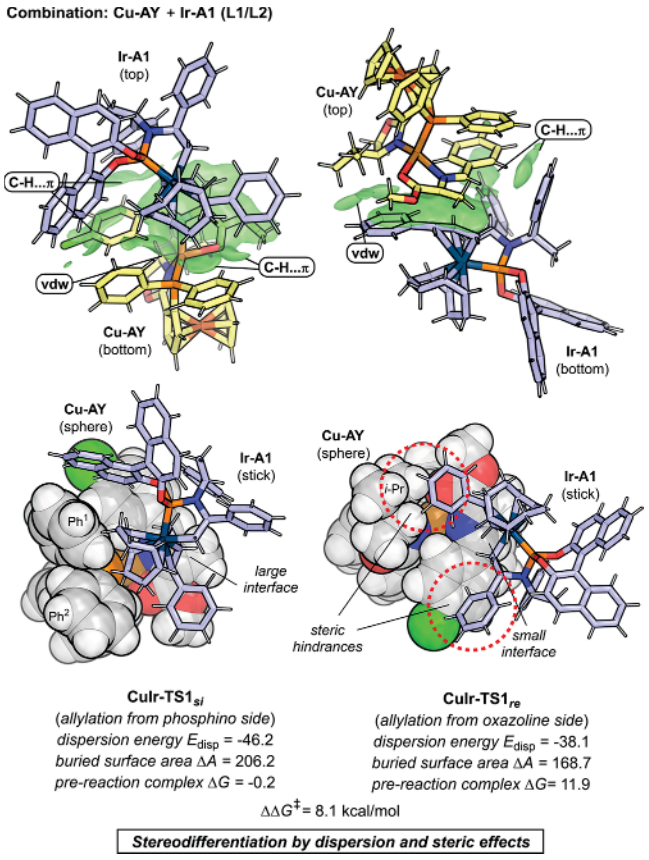

Figure 10. Origin of -center diastereoselectivity in the Cu/Ir system: **CuIr-TS1**$_{si}$ vs **CuIr-TS1**$_{re}$. See caption of Figure 9 for details.

nucleophilic attack of **Ir-A** by **Cu-AY** were studied (Figure 11A). The barriers of **CuIr-TS1** $_{si}$ (with **Ir-A1**) and **CuIr-TS2** $_{si}$ (with **Ir-A2**) are 7.4 and 3.1 kcal/mol higher than **CuIr-TS1**$_{si}$ and **CuIr-TS2**$_{si}$ respectively, which is in accored with the branched selectivity.[17] The preference toward the more substituted allyl terminus (i.e., C3) is typical for Ir-based allylic substitutions.[66,67,70] We studied the origin of regioselectivity using D/I analysis. The analysis ascribes the branched-to-linear selectivity to the smaller interaction energies in branched TSs **CuIr-TS1** $_{si}$ (6.5 kcal/mol lower than than **CuIr-TS1**$_{si}$) and **CuIr-TS2** $_{si}$ (4.2 kcal/mol lower than **CuIr-TS2**$_{si}$, see Figure 11A). Such an interaction-controlled branched-to-linear selectivity differs from the Cu/Pd system and motivated us to examine in Figure 11B the LUMO diagrams of metal allyl species **Ir-A** and **Pd-A**. Interestingly, the LUMO of **Ir-A** displays a greater atomic weight at C3 (20.1 > 4.8 at C1), whereas **Pd-A** exhibits a more symmetrical LUMO distribution (atomic weights: 16.5 at C3 14.3 at C1). The branched selectivity of **Ir-A** can thus arise from the stronger FMO interactions at the C3 site.

4. CONCLUSION

We have reported detailed quantum-mechanical explorations of the mechanisms and origins of enantio-/diastereo-/regioselectivities in the Cu/Pd and Cu/Ir dual-catalytic syntheses of nonproteinogenic , -disubstituted -AAs. The main conclusions are summarized as follows:

Consistent with previous assumptions, we establish a mechanism (Scheme 4) involving the dual activations of aldimine ester and allylic ester to give a nucleophilic copper azomethine ylide and an electrophilic metal π-allyl species. The facile coupling between the pair of in situ formed intermediates yields the desired -AA products. The good agreement with experiments highlights the applicability of quantum mechanical computations for complicated asymmetric processes at a scale of 150 250 atoms.

We showcase the application of a set of analytical tools that proves effective for unveiling the mode of facial discrimination of *N*-metalated azomethine ylide, by far the most employed metal enolate-type prochiral nucleophile in stereodivergent systems. Since there has been limited insight into the asymmetric induction in

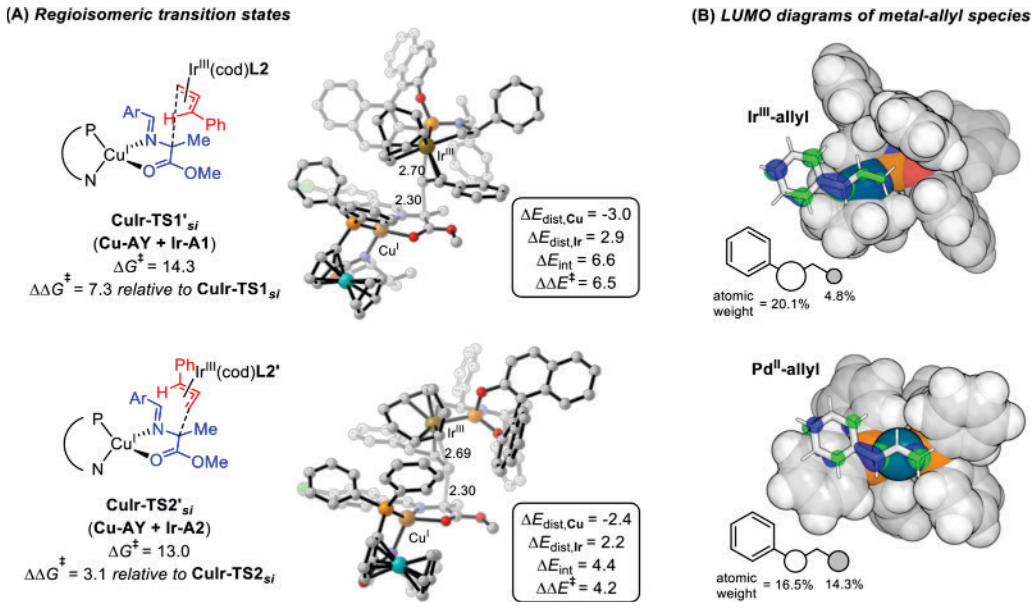

Figure 11. Origin of regioselectivity in the synergistic Cu/Ir system. (A) Regioisomeric transition states affording linear products, with free energy barriers and D/I energies. (B) LUMO diagrams of metal-allyl species.

https://doi.org/10.1021/jacs.1c12664
J. Am. Chem. Soc. 2022 144 1971 1985

Scheme 4. Summary of Catalytic Cycles for Synergistic Pd/Cu and Ir/Cu Catalysis

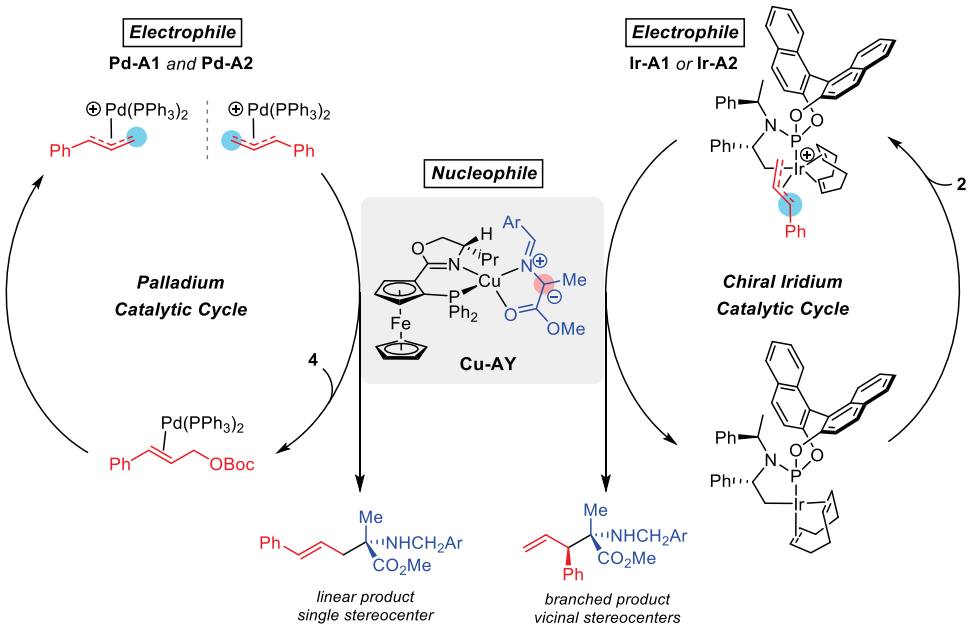

stereodivergent dual transition-metal catalysis, the results provide a framework for rationalizing the stereoselection at the quaternary -stereocenter based on energetic and physical organic parameters. Speci - cally, we show that the stereoselection about the prochiral nucleophile can deviate from the canonical interpretation of stereodivergent dual catalysis,[3] as the mode of facial discrimination is not only determined by the copper catalyst but also depends on the stereo-recognition between the two coupling partners. Moreover, attractive dispersion and sterically caused structural distortions can originate from different aspects of stereorecognition and consequently act under different circumstances. It follows that the nature of stereodivergence can be more involved than usually assumed, and the precise understanding of stereodivergence in relevant synthetic methods in turn comprises a theoretical question for future investigations.

Many preceding studies on stereodivergent dual catalysis focused on the stereocontrolling bond-forming step, which sometimes implicitly applied certain Curtin Hammett condition(s) on certain isomers of the coupling partners. Our computational results support the relative stereochemical stability of metal π-allyl species as compared to the facile bond-forming events. The results indicate that Curtin Hammett conditions might not always hold, especially given the variation of substrates and reaction conditions. This emphasizes a mechanistic parameter for the more precise interpretation and/or catalytic control of these reactions. Notably, the prochiral nucleophile can stereoconvergently intercept a racemic mixture of allylpalladium to afford enantioenriched product in the Cu/Pd dual catalysis, which reflects the robustness of the stereoinduction.

A comparison of the two dual-catalytic systems points to the regiochemical preference of metal π-allyl species to dictate the number of stereocenters. We show that the stronger FMO interactions for the more substituted terminus of allyliridium overcome the steric impediment and thereby render the branched product more favorable in the Cu/Ir system. In contrast, the allylpalladium with a more symmetrical LUMO is subject to a steric control of regiochemistry, hence the linear preference in the Cu/Pd dual catalysis.

In summary, this study not only provides novel molecular insights into the mechanism and asymmetric induction in synergistic dual transition-metal catalysis but also further explores how practical quantum mechanical computations can be analyzed to rationalize complicated organometallic reactions and asymmetric processes involving sizable catalyst architectures.

ASSOCIATED CONTENT

Supporting Information

The Supporting Information is available free of charge at https://pubs.acs.org/doi/10.1021/jacs.1c12664.

Supplementary computations, energetics and coordinates of optimized structures (PDF)

AUTHOR INFORMATION

Corresponding Authors

Yanfeng Dang *Tianjin Key Laboratory of Molecular Optoelectronic Sciences Department of Chemistry School of Science Tianjin University Tianjin 300072 China;* orcid.org/0000-0002-9297-9759; Email: yanfeng.dang@tju.edu.cn

K N Houk *Department of Chemistry and Biochemistry University of California Los Angeles California 90095 United States;* orcid.org/0000-0002-8387-5261; Email: houk@chem.ucla.edu

Authors

Bo Li *Tianjin Key Laboratory of Molecular Optoelectronic Sciences Department of Chemistry School of Science Tianjin University Tianjin 300072 China; Department of Chemistry and Biochemistry University of California Los Angeles California 90095 United States*

https://doi.org/10.1021/jacs.1c12664
J. Am. Chem. Soc. 2022 144 1971 1985

Hui Xu *Tianjin Key Laboratory of Molecular Optoelectronic Sciences Department of Chemistry School of Science Tianjin University Tianjin 300072 China*

Complete contact information is available at: https://pubs.acs.org/10.1021/jacs.1c12664

Notes

The authors declare no competing nancial interest.

ACKNOWLEDGMENTS

We acknowledge support for this work from the National Natural Science Foundation of China (Grant No. 22073067) and the National Science Foundation (Grant No. CHE-1764328). Calculations were performed on the Hoffman2 cluster at the University of California, Los Angeles, and the Extreme Science and Engineering Discovery Environment (XSEDE), which is supported by the National Science Foundation (Grant OCI-1053575).

REFERENCES

(1) (a) Caldwell, J. The Importance of Stereochemistry in Drug Action and Disposition. *J. Clin. Pharmacol.* **1992**, *32*, 925 929. (b) Jozwiak, K.; Lough, W. J.; Wainer, I. W. *Drug Stereochemistry: Analytical Methods and Pharmacology*, 3rd ed.; Informa: New York, 2012. (c) Rentsch, K. M. The Importance of Stereoselective Determination of Drugs in The Clinical Laboratory. *J. Biochem. Biophys. Methods* **2002**, *54*, 1 9.

(2) Selected recent works on transition-metal-catalyzed syntheses of multichiral molecules: (a) Ashida, K.; Hoshimoto, Y.; Tohnai, N.; Scott, D. E.; Ohashi, M.; Imaizumi, H.; Tsuchiya, Y.; Ogoshi, S. Enantioselective Synthesis of Polycyclic γ-Lactams with Multiple Chiral Carbon Centers via Ni(0)-Catalyzed Asymmetric Carbonylative Cycloadditions without Stirring. *J. Am. Chem. Soc.* **2020**, *142*, 1594 1602. (b) Trost, B. M.; Gnanamani, E.; Kalnmals, C. A.; Hung, C.-I.; Tracy, J. S. Direct Enantio- and Diastereoselective Vinylogous Addition of Butenolides to Chromones Catalyzed by Zn-ProPhenol. *J. Am. Chem. Soc.* **2019**, *141*, 1489 1493. (c) Ishihara, H.; Huang, J.; Mochizuki, T.; Hatano, M.; Ishihara, K. Enantio- and Diastereoselective Carbonyl-Ene Cyclization Acetalization Tandem Reaction Catalyzed by Tris(pentafluorophenyl)borane-Assisted Chiral Phosphoric Acids. *ACS Catal.* **2021**, *11*, 6121 6127. (d) Zheng, G.; Zhou, Z.; Zhu, G.; Zhai, S.; Xu, H.; Duan, X.; Yi, W.; Li, X. Rhodium(III)-Catalyzed Enantio- and Diastereoselective C H Cyclopropylation of N-Phenoxylsulfonamides: Combined Experimental and Computational Studies. *Angew. Chem. Int. Ed.* **2020**, *59*, 2890 2896. (e) Matviitsuk, A.; Denmark, S. E. Enantio- and Diastereoselective, Lewis Base Catalyzed, Cascade Sulfenoacetalization of Alkenyl Aldehydes. *Angew. Chem. Int. Ed.* **2019**, *58*, 12486 12490. (f) Manna, S.; Dherbassy, Q.; Perry, G. J. P.; Procter, D. J. Enantio- and Diastereoselective Synthesis of Homopropargyl Amines by Copper-Catalyzed Coupling of Imines, 1,3-Enynes, and Diborons. *Angew. Chem. Int. Ed.* **2020**, *59*, 4879 4882. (g) Han, Y.-Q.; Yang, X.; Kong, K.-X.; Deng, Y.-T.; Wu, L.-S.; Ding, Y.; Shi, B.-F. Synthesis of Acyclic Aliphatic Amides with Contiguous Stereogenic Centers via Palladium-Catalyzed Enantio-, Chemo- and Diastereoselective Methylene C(sp^3) H arylation. *Angew. Chem. Int. Ed.* **2020**, *59*, 20455 20458.

(3) (a) Krautwald, S.; Sarlah, D.; Schafroth, M. A.; Carreira, E. M. Enantio- and Diastereodivergent Dual Catalysis: -Allylation of Branched Aldehydes. *Science* **2013**, *340*, 1065 1068. (b) For a related perspective, see: Schindler, C. S.; Jacobsen, E. N. A New Twist on Cooperative Catalysis. *Science* **2013**, *340*, 1052 1053.

(4) Selected recent reviews/perspectives on stereodivergent dual catalysis: (a) Bihani, M.; Zhao, J. C.-G. Advances in Asymmetric Diastereodivergent Catalysis. *Adv. Synth. Catal.* **2017**, *359*, 534 575. (b) Krautwald, S.; Carreira, E. M. Stereodivergence in Asymmetric Catalysis. *J. Am. Chem. Soc.* **2017**, *139*, 5627 5639. (c) Beletskaya, I. P.; Nájera, C.; Yus, M. Stereodivergent Catalysis. *Chem. Rev.* **2018**, *118*, 5080 5200. (d) Kalita, S. J.; Huang, Y.-Y.; Schneider, U. Stereodivergent Catalytic Asymmetric Allylic Alkylation. *Science Bulletin* **2020**, *65*, 1865 1868. (e) Martínez, S.; Veth, L.; Lainer, B.; Dydio, P. Challenges and Opportunities in Multicatalysis. *ACS Catal.* **2021**, *11*, 3891 3915.

(5) (a) Krautwald, S.; Schafroth, M. A.; Sarlah, D.; Carreira, E. M. Stereodivergent -Allylation of Linear Aldehydes with Dual Iridium and Amine Catalysis. *J. Am. Chem. Soc.* **2014**, *136*, 3020 3023. (b) Schafroth, M. A.; Zuccarello, G.; Krautwald, S.; Sarlah, D.; Carreira, E. M. Stereodivergent Total Synthesis of ^{9}-Tetrahydrocannabinols. *Angew. Chem. Int. Ed.* **2014**, *53*, 13898 13901. (c) Sandmeier, T.; Krautwald, S.; Zipfel, H. F.; Carreira, E. M. Stereodivergent Dual Catalytic -Allylation of Protected -Amino- and -Hydroxyacetaldehydes. *Angew. Chem. Int. Ed.* **2015**, *54*, 14363 14367.

(6) Naesborg, L.; Halskov, K. S.; Tur, F.; Mønsted, S. M. N.; Jørgensen, K. A. Asymmetric γ-Allylation of ,β-Unsaturated Aldehydes by Combined Organocatalysis and Transition-Metal Catalysis. *Angew. Chem. Int. Ed.* **2015**, *54*, 10193 10197.

(7) Jiang, X.; Beiger, J. J.; Hartwig, J. F. Stereodivergent Allylic Substitutions with Aryl Acetic Acid Esters by Synergistic Iridium and Lewis Base Catalysis. *J. Am. Chem. Soc.* **2017**, *139*, 87 90.

(8) Cruz, F. A.; Dong, V. M. Stereodivergent Coupling of Aldehydes and Alkynes via Synergistic Catalysis Using Rh and Jacobsen s Amine. *J. Am. Chem. Soc.* **2017**, *139*, 1029 1032.

(9) Singha, S.; Serrano, E.; Mondal, S.; Daniliuc, C. G.; Glorius, F. Diastereodivergent Synthesis of Enantioenriched ,β-Disubstituted γ-Butyrolactones via Cooperative N-Heterocyclic Carbene and Ir Catalysis. *Nat. Catal.* **2020**, *3*, 48 54.

(10) Zhang, M.-M.; Wang, Y.-N.; Wang, B.-C.; Chen, X.-W.; Lu, L.-Q.; Xiao, W.-J. Synergetic Iridium and Amine Catalysis Enables Asymmetric [4 + 2] Cycloadditions of Vinyl Aminoalcohols with Carbonyls. *Nat. Commun.* **2019**, *10*, 2716.

(11) Zhang, J.; Gao, Y.-S.; Gu, B.-M.; Yang, W.-L.; Tian, B.-X.; Deng, W.-P. Cooperative N-heterocyclic Carbene and Iridium Catalysis Enables Stereoselective and Regiodivergent [3 + 2] and [3 + 3] Annulation Reactions. *ACS Catal.* **2021**, *11*, 3810 3821.

(12) Huo, X.; He, R.; Zhang, X.; Zhang, W. An Ir/Zn Dual Catalysis for Enantio- and Diastereodivergent -Allylation of -Hydroxyketones. *J. Am. Chem. Soc.* **2016**, *138*, 11093 11096.

(13) For selected reviews, see: (a) Fu, J.; Huo, X.; Li, B.; Zhang, W. Cooperative Bimetallic Catalysis in Asymmetric Allylic Substitution. *Org. Biomol. Chem.* **2017**, *15*, 9747 9759. (b) Kim, U. B.; Jung, D. J.; Jeon, H. J.; Rathwell, K.; Lee, S.-G. Synergistic Dual Transition Metal Catalysis. *Chem. Rev.* **2020**, *120*, 13382 13433.

(14) He, R.; Liu, P.; Huo, X.; Zhang, W. Ir/Zn Dual Catalysis: Enantioselective and Diastereodivergent -Allylation of Unprotected -Hydroxy Indanones. *Org. Lett.* **2017**, *19*, 5513 5516.

(15) Huo, X.; Zhang, J.; Fu, J.; He, R.; Zhang, W. Ir/Cu Dual Catalysis: Enantio- and Diastereodivergent Access to , -Disubstituted -Amino Acids Bearing Vicinal Stereocenters. *J. Am. Chem. Soc.* **2018**, *140*, 2080 2084.

(16) (a) He, R.; Huo, X.; Zhao, L.; Wang, F.; Jiang, L.; Liao, J.; Zhang, W. Stereodivergent Pd/Cu Catalysis for the Dynamic Kinetic Asymmetric Transformation of Racemic Unsymmetrical 1,3-Disubstituted Allyl Acetates. *J. Am. Chem. Soc.* **2020**, *142*, 8097 8103. (b) Zhang, J.; Huo, X.; Li, B.; Chen, Z.; Zou, Y.; Sun, Z.; Zhang, W. Enantioselective and Diastereodivergent Access to -Substituted -Amino Acids via Dual Iridium and Copper Catalysis. *Adv. Synth. Catal.* **2019**, *361*, 1130 1139. (c) Zhao, L.; Li, G.; He, R.; Liu, P.; Wang, F.; Huo, X.; Zhao, M.; Zhang, W. Stereodivergent Pd/Cu Catalysis: Asymmetric Alkylation of Racemic Symmetrical 1,3-Diphenyl Allyl Acetates. *Org. Biomol. Chem.* **2021**, *19*, 1955 1959. (d) Huo, X.; Zhao, L.; Luo, Y.; Wu, Y.; Sun, Y.; Li, G.; Gridneva, T.; Zhang, J.; Ye, Y.; Zhang, W. Stereodivergent Pd/Cu Catalysis for Asymmetric Desymmetric Alkylation of Allylic Geminal Dicarboxylates. *CCS Chem.* **2021**, *3*, 1933 1944. (e) Xia, J.; Hirai, T.;

Katayama, S.; Nagae, H.; Zhang, W.; Mashima, K. Mechanistic Study of Ni and Cu Dual Catalyst for Asymmetric C C Bond Formation; Asymmetric Coupling of 1,3-Dienes with C-nucleophiles to Construct Vicinal Stereocenters. *ACS Catal.* **2021**, *11*, 6643 6655. (f) Zhang, J.; Huo, X.; Xiao, J.; Zhao, L.; Ma, S.; Zhang, W. Enantio- and Diastereodivergent Construction of 1,3-Nonadjacent Stereocenters Bearing Axial and Central Chirality through Synergistic Pd/Cu Catalysis. *J. Am. Chem. Soc.* **2021**, *143*, 12622 12632.

(17) Wei, L.; Zhu, Q.; Xu, S.-M.; Chang, X.; Wang, C.-J. Stereodivergent Synthesis of , -Disubstituted -Amino Acids via Synergistic Cu/Ir Catalysis. *J. Am. Chem. Soc.* **2018**, *140*, 1508 1513.

(18) (a) Xu, S.-M.; Wei, L.; Shen, C.; Xiao, L.; Tao, H.-Y.; Wang, C.-J. Stereodivergent Assembly of Tetrahydro-γ-carbolines via Synergistic Catalytic Asymmetric Cascade Reaction. *Nat. Commun.* **2019**, *10*, 5553. (b) Wei, L.; Zhu, Q.; Xiao, L.; Tao, H.-Y.; Wang, C.-J. Synergistic Catalysis for Cascade Allylation and 2-Aza-Cope Rearrangement of Azomethine Ylides. *Nat. Commun.* **2019**, *10*, 1594. (c) Wu, H.-M.; Zhang, Z.; Xiao, F.; Wei, L.; Dong, X.-Q.; Wang, C.-J. Stereodivergent Synthesis of -Quaternary Serine and Cysteine Derivatives Containing Two Contiguous Stereogenic Centers via Synergistic Cu/Ir Catalysis. *Org. Lett.* **2020**, *22*, 4852 4857.

(19) (a) He, Z.-T.; Jiang, X.; Hartwig, J. F. Stereodivergent Construction of Tertiary Fluorides in Vicinal Stereogenic Pairs by Allylic Substitution with Iridium and Copper Catalysts. *J. Am. Chem. Soc.* **2019**, *141*, 13066 13073. (b) Jiang, X.; Boehm, P.; Hartwig, J. F. Stereodivergent Allylation of Azaaryl Acetamides and Acetates by Synergistic Iridium and Copper Catalysis. *J. Am. Chem. Soc.* **2018**, *140*, 1239 1242.

(20) (a) Zhang, Q.; Yu, H.; Shen, L.; Tang, T.; Dong, D.; Chai, W.; Zi, W. Stereodivergent Coupling of 1,3-Dienes with Aldimine Esters Enabled by Synergistic Pd and Cu Catalysis. *J. Am. Chem. Soc.* **2019**, *141*, 14554 14559. (b) Zhu, M.; Zhang, Q.; Zi, W. Diastereodivergent Synthesis of β-Amino Alcohols by Dual-Metal-Catalyzed Coupling of Alkoxyallenes with Aldimine Esters. *Angew. Chem. Int. Ed.* **2021**, *60*, 6545 6552.

(21) Yang, S.-Q.; Wang, Y.-F.; Zhao, W.-C.; Lin, G.-Q.; He, Z.-T. Stereodivergent Synthesis of Tertiary Fluoride-Tethered Allenes via Copper and Palladium Dual Catalysis. *J. Am. Chem. Soc.* **2021**, *143*, 7285 7291.

(22) (a) Bhaskararao, B.; Sunoj, R. B. Origin of Stereodivergence in Cooperative Asymmetric Catalysis with Simultaneous Involvement of Two Chiral Catalysts. *J. Am. Chem. Soc.* **2015**, *137*, 15712 15722. (b) Bhaskararao, B.; Sunoj, R. B. Asymmetric Dual Chiral Catalysis using Iridium Phosphoramidites and Diarylprolinol Silyl Ethers: Insights into Stereodivergence. *ACS Catal.* **2017**, *7*, 6675 6685. (c) Tribedi, S.; Hadad, C. M.; Sunoj, R. B. Origin of Stereoselectivity in the Amination of Alcohols using Cooperative Asymmetric Dual Catalysis Involving Chiral Counter-Ions. *Chem. Sci.* **2018**, *9*, 6126 6133. (d) Bhaskararao, B.; Sunoj, R. B. Two Chiral Catalysts in Action: Insights into Cooperativity and Stereoselectivity in Proline and Cinchona-Thiourea Dual Organocatalysis. *Chem. Sci.* **2018**, *9*, 8738 8747.

(23) Selected theoretical studies concerning achiral dual transition-metal-catalyzed transformations: (a) Kalek, M.; Himo, F. Mechanism and Selectivity of Cooperatively Catalyzed Meyer Schuster Rearrangement/Tsuji Trost Allylic Substitution. Evaluation of Synergistic Catalysis by Means of Combined DFT and Kinetics Simulations. *J. Am. Chem. Soc.* **2017**, *139*, 10250 10266. (b) Funes-Ardoiz, I.; Maseras, F. Cooperative Reductive Elimination: The Missing Piece in the Oxidative-Coupling Mechanistic Puzzle. *Angew. Chem. Int. Ed.* **2016**, *55*, 2764 2767. (c) Funes-Ardoiz, I.; Maseras, F. Computational Characterization of the Mechanism for the Oxidative Coupling of Benzoic Acid and Alkynes by Rhodium/Copper and Rhodium/Silver systems. *Chem. - Eur. J.* **2018**, *24*, 12383 12388. For related recent reviews, see: (d) Sciortino, G.; Maseras, F. Computational Study of Homogeneous Multimetallic Cooperative Catalysis. *Top. Catal.* **2021**, DOI: 10.1007/s11244-021-01493-2. (e) Matsuzawa, A.; Harvey, J. N.; Himo, F. On the Importance of Considering Multinuclear Metal Sites in Homogeneous Catalysis Modeling. *Top. Catal.* **2021**, DOI: 10.1007/s11244-021-01507-z.

(24) Changotra, A.; Bhaskararao, B.; Hadad, C. M.; Sunoj, R. B. Insights on Absolute and Relative Stereocontrol in Stereodivergent Cooperative Catalysis. *J. Am. Chem. Soc.* **2020**, *142*, 9612 9624.

(25) Xu, H.; Li, B.; Liu, Z.; Dang, Y. Mechanistic Origins of Stereodivergence in Asymmetric Cascade Allylation and Cyclization Reactions Enabled by Synergistic Cu/Ir Catalysis. *ACS Catal.* **2021**, *11*, 9008 9021.

(26) Selected recent developments of chiral organometallic catalysts based on dispersion interactions: (a) Singha, S.; Buchsteiner, M.; Bistoni, G.; Goddard, R.; Fürstner, A. A New Ligand Design Based on London Dispersion Empowers Chiral Bismuth Rhodium Paddlewheel Catalysts. *J. Am. Chem. Soc.* **2021**, *143*, 5666 5673. (b) Chen, J.; Gridnev, I. D. Size is Important: Artificial Catalyst Mimics Behavior of Natural Enzymes. *iScience* **2020**, *23*, 100960. (c) Xi, Y.; Su, B.; Qi, X.; Pedram, S.; Liu, P.; Hartwig, J. F. Application of Trimethylgermanyl-Substituted Bisphosphine Ligands with Enhanced Dispersion Interactions to Copper-Catalyzed Hydroboration of Disubstituted Alkenes. *J. Am. Chem. Soc.* **2020**, *142*, 18213 18222. (d) Wang, H.; Park, Y.; Bai, Z.; Chang, S.; He, G.; Chen, G. Iridium-Catalyzed Enantioselective C(sp^3) H Amidation Controlled by Attractive Noncovalent Interactions. *J. Am. Chem. Soc.* **2019**, *141*, 7194 7201.

(27) Other selected recent studies on organometallic stereoinduction: (a) Eschmann, C.; Song, L.; Schreiner, P. R. London Dispersion Interactions Rather than Steric Hindrance Determine the Enantioselectivity of the Corey Bakshi Shibata Reduction. *Angew. Chem. Int. Ed.* **2021**, *60*, 4823 4832. (b) Deng, L.; Fu, Y.; Lee, S. Y.; Wang, C.; Liu, P.; Dong, G. Kinetic Resolution via Rh-Catalyzed C C Activation of Cyclobutanones at Room Temperature. *J. Am. Chem. Soc.* **2019**, *141*, 16260 16265. (c) Li, B.; Chen, J.; Zhang, Z.; Gridnev, I. D.; Zhang, W. Nickel-Catalyzed Asymmetric Hydrogenation of N-Sulfonyl Imines. *Angew. Chem. Int. Ed.* **2019**, *58*, 7329 7334. (d) Gridnev, I. D. Attraction versus Repulsion in Rhodium-Catalyzed Asymmetric Hydrogenation. *ChemCatChem.* **2016**, *8*, 3463 3468. (e) Wang, T.; Zhuo, L.-G.; Li, Z.; Chen, F.; Ding, Z.; He, Y.; Fan, Q.-H.; Xiang, J.; Yu, Z.-X.; Chan, A. S. C. Highly Enantioselective Hydrogenation of Quinolines Using Phosphine-Free Chiral Cationic Ruthenium Catalysts: Scope, Mechanism, and Origin of Enantioselectivity. *J. Am. Chem. Soc.* **2011**, *133*, 9878 9891.

(28) Selected studies for dispersion effects on other types of organometallic catalysis: (a) Saper, N. I.; Ohgi, A.; Small, D. W.; Semba, K.; Nakao, Y.; Hartwig, J. F. Nickel-Catalysed *anti*-Markovnikov Hydroarylation of Unactivated Alkenes with Unactivated Arenes Facilitated by Non-Covalent Interactions. *Nat. Chem.* **2020**, *12*, 276 283. (b) Kalvet, I.; Deckers, K.; Funes-Ardoiz, I.; Magnin, G.; Sperger, T.; Kremer, M.; Schoenebeck, F. Selective *ortho*-Functionalization of Adamantylarenes Enabled by Dispersion and an Air-Stable Palladium(I) Dimer. *Angew. Chem. Int. Ed.* **2020**, *59*, 7721 7725. (c) Thomas, A. A.; Speck, K.; Kevlishvili, I.; Lu, Z.; Liu, P.; Buchwald, S. L. Mechanistically Guided Design of Ligands That Significantly Improve the Efficiency of CuH-Catalyzed Hydroamination Reactions. *J. Am. Chem. Soc.* **2018**, *140*, 13976 13984. (d) Chen, J.; Zhang, Z.; Li, B.; Li, F.; Wang, Y.; Zhao, M.; Gridnev, I. D.; Imamoto, T.; Zhang, W. $Pd(OAc)_2$-Catalyzed Asymmetric Hydrogenation of Sterically Hindered N-tosylimines. *Nat. Commun.* **2018**, *9*, 5000. (e) Lu, G.; Liu, R. Y.; Yang, Y.; Fang, C.; Lambrecht, D. S.; Buchwald, S. L.; Liu, P. Ligand Substrate Dispersion Facilitates the Copper-Catalyzed Hydroamination of Unactivated Olefins. *J. Am. Chem. Soc.* **2017**, *139*, 16548 16555. (f) Meyer, T. H.; Liu, W.; Feldt, M.; Wuttke, A.; Mata, R. A.; Ackermann, L. Manganese(I)-Catalyzed Dispersion-Enabled C-H/C-C Activation. *Chem. Eur. J.* **2017**, *23*, 5443 5447. (g) Lyngvi, E.; Sanhueza, I. A.; Schoenebeck, F. Dispersion Makes the Difference: Bisligated Transition States Found for the Oxidative Addition of $Pd(PtBu_3)_2$ to Ar-OSO_2R and Dispersion-Controlled Chemoselectivity in Reactions with $Pd[P(iPr)(tBu_2)]_2$. *Organometallics* **2015**, *34*, 805 812. (h) Lu, Q.; Neese, F.; Bistoni, G. London Dispersion Effects in the Coordination and

Activation of Alkanes in σ-complexes: A Local Energy Decomposition Study. *Phys. Chem. Chem. Phys.* **2019**, *21*, 11569 11577.
(29) For related perspectives/reviews, see: (a) Knowles, R. R.; Jacobsen, E. N. Attractive Noncovalent Interactions in Asymmetric Catalysis: Links between Enzymes and Small Molecule Catalysts. *Proc. Natl. Acad. Sci. U. S. A.* **2010**, *107*, 20678 20685. (b) Wagner, J. P.; Schreiner, P. R. London Dispersion in Molecular Chemistry Reconsidering Steric Effects. *Angew. Chem. Int. Ed.* **2015**, *54*, 12274 12296. (c) Sperger, T.; Sanhueza, I. A.; Schoenebeck, F. Computation and Experiment: A Powerful Combination to Understand and Predict Reactivities. *Acc. Chem. Res.* **2016**, *49*, 1311 1319. (d) Liptrot, D. J.; Power, P. P. London Dispersion Forces in Sterically Crowded Inorganic and Organometallic Molecules. *Nat. Rev. Chem.* **2017**, *1*, 0004. (e) Bursch, M.; Caldeweyher, E.; Hansen, A.; Neugebauer, H.; Ehlert, S.; Grimme, S. Understanding and Quantifying London Dispersion Effects in Organometallic Complexes. *Acc. Chem. Res.* **2019**, *52*, 258 266. (f) Fanourakis, A.; Docherty, P. J.; Chuentragool, P.; Phipps, R. J. Recent Developments in Enantioselective Transition Metal Catalysis Featuring Attractive Noncovalent Interactions between Ligand and Substrate. *ACS Catal.* **2020**, *10*, 10672 10714.
(30) Wei, L.; Xu, S.-M.; Zhu, Q.; Che, C.; Wang, C.-J. Synergistic Cu/Pd Catalysis for Enantioselective Allylic Alkylation of Aldimine Esters: Access to , -Disubstituted -Amino Acids. *Angew. Chem. Int. Ed.* **2017**, *56*, 12312 12316.
(31) For selected relevant recent studies, see: (a) Wei, L.; Lu, X.; Wang, C.-J. Synergistic Cu/Pd Catalysis for Enantioselective Allylation of Ketimine Esters: The Direct Synthesis of -Substituted -Amino Acids and 2H-Pyrrols. *Adv. Synth. Catal.* **2018**, *360*, 4715 4719. (b) Huo, X.; He, R.; Fu, J.; Zhang, J.; Yang, G.; Zhang, W. Stereoselective and Site-Specific Allylic Alkylation of Amino Acids and Small Peptides via a Pd/Cu Dual Catalysis. *J. Am. Chem. Soc.* **2017**, *139*, 9819 9822. (c) Xia, J.; Hirai, T.; Katayama, S.; Nagae, H.; Zhang, W.; Mashima, K. Mechanistic Study of Ni and Cu Dual Catalyst for Asymmetric C C Bond Formation; Asymmetric Coupling of 1,3-Dienes with C-nucleophiles to Construct Vicinal Stereocenters. *ACS Catal.* **2021**, *11*, 6643 6655. (d) Liu, P.; Huo, X.; Li, B.; He, R.; Zhang, J.; Wang, T.; Xie, F.; Zhang, W. Stereoselective Allylic Alkylation of 1-Pyrroline-5-carboxylic Esters via a Pd/Cu Dual Catalysis. *Org. Lett.* **2018**, *20*, 6564 6568. (e) Huo, X.; Fu, J.; He, X.; Chen, J.; Xie, F.; Zhang, W. Pd/Cu Dual Catalysis: Highly Enantioselective Access to -Substituted -Amino Acids and -Amino Amides. *Chem. Commun.* **2018**, *54*, 599 602. (f) Xu, S.; Zhang, Z.-M.; Xu, B.; Liu, B.; Liu, Y.; Zhang, J. Enantioselective Regiodivergent Synthesis of Chiral Pyrrolidines with Two Quaternary Stereocenters via Ligand-Controlled Copper(I)-Catalyzed Asymmetric 1,3-Dipolar Cycloadditions. *J. Am. Chem. Soc.* **2018**, *140*, 2272 2283.
(32) For selected reviews related to dual catalysis combining chiral/achiral catalysts: (a) Afewerki, S.; Córdova, A. Combinations of Aminocatalysts and Metal Catalysts: A Powerful Cooperative Approach in Selective Organic Synthesis. *Chem. Rev.* **2016**, *116*, 13512 13570. (b) Inamdar, S. M.; Shinde, V. S.; Patil, N. T. Enantioselective Cooperative Catalysis. *Org. Biomol. Chem.* **2015**, *13*, 8116 8162. (c) Allen, A. E.; MacMillan, D. W. C. Synergistic Catalysis: A Powerful Synthetic Strategy for new Reaction Development. *Chem. Sci.* **2012**, *3*, 633 658. (d) Du, Z.; Shao, Z. Combining Transition Metal Catalysis and Organocatalysis An Update. *Chem. Soc. Rev.* **2013**, *42*, 1337 1378. (e) Shao, Z.; Zhang, H. Combining Transition Metal Catalysis and Organocatalysis: A Broad New Concept for Catalysis. *Chem. Soc. Rev.* **2009**, *38*, 2745 2755.
(33) Wei, L.; Chang, X.; Wang, C.-J. Catalytic Asymmetric Reactions with *N*-Metallated Azomethine Ylides. *Acc. Chem. Res.* **2020**, *53*, 1084 1100.
(34) Wei, L.; Wang, C.-J. Synergistic Catalysis with Azomethine Ylides. *Chin. J. Chem.* **2021**, *39*, 15 24.
(35) Frisch, M. J.; Trucks, G. W.; Schlegel, H. B.; Scuseria, G. E.; Robb, M. A.; Cheeseman, J. R.; Scalmani, G.; Barone, V.; Mennucci, B.; Petersson, G. A.; Nakatsuji, H.; Caricato, M.; Li, X.; Hratchian, H. P.; Izmaylov, A. F.; Bloino, J.; Zheng, G.; Sonnenberg, J. L.; Hada, M.; Ehara, M.; Toyota, K.; Fukuda, R.; Hasegawa, J.; Ishida, M.; Nakajima, T.; Honda, Y.; Kitao, O.; Nakai, H.; Vreven, T.; Montgomery, J. A., Jr.; Peralta, J. E.; Ogliaro, F.; Bearpark, M.; Heyd, J. J.; Brothers, E.; Kudin, K. N.; Staroverov, V. N.; Keith, T.; Kobayashi, R.; Normand, J.; Raghavachari, K.; Rendell, A.; Burant, J. C.; Iyengar, S. S.; Tomasi, J.; Cossi, M.; Rega, N.; Millam, J. M.; Klene, M.; Knox, J. E.; Cross, J. B.; Bakken, V.; Adamo, C.; Jaramillo, J.; Gomperts, R.; Stratmann, R. E.; Yazyev, O.; Austin, A. J.; Cammi, R.; Pomelli, C.; Ochterski, J. W.; Martin, R. L.; Morokuma, K.; Zakrzewski, V. G.; Voth, G. A.; Salvador, P.; Dannenberg, J. J.; Dapprich, S.; Daniels, A. D.; Farkas, O.; Foresman, J. B.; Ortiz, J. V.; Cioslowski, J.; Fox, D. J. *Gaussian 09*; Gaussian, Inc.: Wallingford, CT, 2013.
(36) (a) Zhao, Y.; Truhlar, D. G. A New Local Density Functional for Main-Group Thermochemistry, Transition Metal Bonding, Thermochemical Kinetics, and Noncovalent Interactions. *J. Chem. Phys.* **2006**, *125*, 194101. (b) Zhao, Y.; Truhlar, D. G. The M06 Suite of Density Functionals for Main Group Thermochemistry, Thermochemical Kinetics, Noncovalent Interactions, Excited States, and Transition Elements: Two New Functionals and Systematic Testing of Four M06-Class Functionals and 12 Other Functionals. *Theor. Chem. Acc.* **2008**, *120*, 215 241. (c) Zhao, Y.; Truhlar, D. G. Density Functionals with Broad Applicability in Chemistry. *Acc. Chem. Res.* **2008**, *41*, 157 167.
(37) (a) Andrae, D.; Häussermann, U.; Dolg, M.; Stoll, H.; Preuss, H. Energy-Adjusted ab Initio Pseudopotentials for the Second and Third Row Transition Elements. *Theor. Chim. Acta* **1990**, *77*, 123 141. (b) Roy, L. E.; Hay, P. J.; Martin, R. L. Revised Basis Sets for the LANL Effective Core Potentials. *J. Chem. Theory Comput.* **2008**, *4*, 1029 1031.
(38) Weigend, F.; Ahlrichs, R. Balanced Basis Sets of Split Valence, Triple Zeta Valence and Quadruple Zeta Valence Quality for H to Rn: Design and Assessment of Accuracy. *Phys. Chem. Chem. Phys.* **2005**, *7*, 3297 3305.
(39) Marenich, A. V.; Cramer, C. J.; Truhlar, D. G. Universal Solvation Model Based on Solute Electron Density and on a Continuum Model of the Solvent Defined by the Bulk Dielectric Constant and Atomic Surface Tensions. *J. Phys. Chem. B* **2009**, *113*, 6378 6396.
(40) Luchini, G.; Alegre-Requena, J. V.; Funes-Ardoiz, I.; Paton, R. S. GoodVibes: Automated Thermochemistry for Heterogeneous Computational Chemistry Data. *F1000Res.* **2020**, *9*, 291.
(41) (a) Grimme, S. Supramolecular Binding Thermodynamics by Dispersion-Corrected Density Functional Theory. *Chem. -Eur. J.* **2012**, *18*, 9955 9964. (b) Li, Y.-P.; Gomes, J.; Sharada, S. M.; Bell, A. T.; Head-Gordon, M. Improved Force-Field Parameters for QM/MM Simulations of the Energies of Adsorption for Molecules in Zeolites and a Free Rotor Correction to the Rigid Rotor Harmonic Oscillator Model for Adsorption Enthalpies. *J. Phys. Chem. C* **2015**, *119*, 1840 1850.
(42) (a) Horn, P. R.; Mao, Y.; Head-Gordon, M. Probing Non-Covalent Interactions with a Second Generation Energy Decomposition Analysis using Absolutely Localized Molecular Orbitals. *Phys. Chem. Chem. Phys.* **2016**, *18*, 23067 23079. (b) Horn, P. R.; Mao, Y.; Head-Gordon, M. Defining the Contributions of Permanent Electrostatics, Pauli Repulsion, and Dispersion in Density Functional Theory Calculations of Intermolecular Interaction Energies. *J. Chem. Phys.* **2016**, *144*, 114107. (c) Horn, P. R.; Head-Gordon, M. Polarization Contributions to Intermolecular Interactions Revisited with Fragment Electric-Field Response Functions. *J. Chem. Phys.* **2015**, *143*, 114111.
(43) Shao, Y.; Gan, Z.; Epifanovsky, E.; Gilbert, A. T. B.; Wormit, M.; Kussmann, J.; Lange, A. W.; Behn, A.; Deng, J.; Feng, X.; Ghosh, D.; Goldey, M.; Horn, P. R.; Jacobson, L. D.; Kaliman, I.; Khaliullin, R. Z.; Kus, T.; Landau, A.; Liu, J.; Proynov, E. I.; Rhee, Y. M.; Richard, R. M.; Rohrdanz, M. A.; Steele, R. P.; Sundstrom, E. J.; Woodcock, H. L., III; Zimmerman, P. M.; Zuev, D.; Albrecht, B.; Alguire, E.; Austin, B.; Beran, G. J. O.; Bernard, Y. A.; Berquist, E.; Brandhorst, K.; Bravaya, K. B.; Brown, S. T.; Casanova, D.; Chang, C.-M.; Chen, Y.; Chien, S. H.; Closser, K. D.; Crittenden, D. L.;

https://doi.org/10.1021/jacs.1c12664
J. Am. Chem. Soc. 2022 144 1971 1985

Diedenhofen, M.; DiStasio, R. A.; Do, H.; Dutoi, A. D.; Edgar, R. G.; Fatehi, S.; Fusti-Molnar, L.; Ghysels, A.; Golubeva-Zadorozhnaya, A.; Gomes, J.; Hanson-Heine, M. W. D.; Harbach, P. H. P.; Hauser, A. W.; Hohenstein, E. G.; Holden, Z. C.; Jagau, T.-C.; Ji, H.; Kaduk, B.; Khistyaev, K.; Kim, J.; Kim, J.; King, R. A.; Klunzinger, P.; Kosenkov, D.; Kowalczyk, T.; Krauter, C. M.; Lao, K. U.; Laurent, A. D.; Lawler, K. V.; Levchenko, S. V.; Lin, C. Y.; Liu, F.; Livshits, E.; Lochan, R. C.; Luenser, A.; Manohar, P.; Manzer, S. F.; Mao, S.-P.; Mardirossian, N.; Marenich, A. V.; Maurer, S. A.; Mayhall, N. J.; Neuscamman, E.; Oana, C. M.; Olivares-Amaya, R.; O Neill, D. P.; Parkhill, J. A.; Perrine, T. M.; Peverati, R.; Prociuk, A.; Rehn, D. R.; Rosta, E.; Russ, N. J.; Sharada, S. M.; Sharma, S.; Small, D. W.; Sodt, A.; Stein, T.; Stück, D.; Su, Y.-C.; Thom, A. J. W.; Tsuchimochi, T.; Vanovschi, V.; Vogt, L.; Vydrov, O.; Wang, T.; Watson, M. A.; Wenzel, J.; White, A.; Williams, C. F.; Yang, J.; Yeganeh, S.; Yost, S. R.; You, Z.-Q.; Zhang, I. Y.; Zhang, X.; Zhao, Y.; Brooks, B. R.; Chan, G. K.-L.; Chipman, D. M.; Cramer, C. J.; Goddard, W. A., III; Gordon, M. S.; Hehre, W. J.; Klamt, A.; Henry, F. S., III; Schmidt, M. W.; Sherrill, C. D.; Truhlar, D. G.; Warshel, A.; Xu, X.; Aspuru-Guzik, A.; Baer, R.; Bell, A. T.; Besley, N. A.; Chai, J.-D.; Dreuw, A.; Dunietz, B. D.; Furlani, T. R.; Gwaltney, S. R.; Hsu, C.-P.; Jung, Y.; Kong, J.; Lambrecht, D. S.; Liang, W.; Ochsenfeld, C.; Rassolov, V. A.; Slipchenko, L. V.; Subotnik, J. E.; Van Voorhis, T.; Herbert, J. M.; Krylov, A. I.; Gill, P. M. W.; Head-Gordon, M. Advances in molecular quantum chemistry contained in the Q-Chem 4 program package. *Mol. Phys.* **2015**, *113*, 184 215.

(44) Lu, T.; Chen, F. Multiwfn: A Multifunctional Wavefunction Analyzer. *J. Comput. Chem.* **2012**, *33*, 580 592.

(45) Liu, P.; Montgomery, J.; Houk, K. N. Ligand Steric Contours To Understand the Effects of N-Heterocyclic Carbene Ligands on the Reversal of Regioselectivity in Ni-Catalyzed Reductive Couplings of Alkynes and Aldehydes. *J. Am. Chem. Soc.* **2011**, *133*, 6956 6959.

(46) Lu, T.; Chen, F. Quantitative Analysis of Molecular Surface Based on Improved Marching Tetrahedra Algorithm. *J. Mol. Graph. Model.* **2012**, *38*, 314 323.

(47) Lu, T.; Chen, Q. van der Waals Potential: An Important Complement to Molecular Electrostatic Potential in Studying Intermolecular Interactions. *J. Mol. Model.* **2020**, *26*, 315.

(48) Lefebvre, C.; Rubez, G.; Khartabil, H.; Boisson, J.-C.; Contreras-García, J.; Hénon, E. Accurately Extracting the Signature of Intermolecular Interactions Present in the NCI Plot of the Reduced Density Gradient versus Electron Density. *Phys. Chem. Chem. Phys.* **2017**, *19*, 17928 17936.

(49) (a) Legault, C. Y. *CYLview 1.0b*; Université de Sherbrooke: Quebec, Montreal, Canada, 2009. (b) Delano, W. L. *The PyMOL Molecular Graphics System*; Delano Scienti c, 2002.

(50) (a) Chang, X.; Yang, Y.; Shen, C.; Xue, K.-S.; Wang, Z.-F.; Cong, H.; Tao, H.-Y.; Chung, L. W.; Wang, C.-J. β-Substituted Alkenyl Heteroarenes as Dipolarophiles in the Cu(I)-Catalyzed Asymmetric 1,3-Dipolar Cycloaddition of Azomethine Ylides Empowered by a Dual Activation Strategy: Stereoselectivity and Mechanistic Insight. *J. Am. Chem. Soc.* **2021**, *143*, 3519 3535. (b) Shen, C.; Yang, Y.; Wei, L.; Dong, W.-W.; Chung, L. W.; Wang, C.-J. Kinetic Resolution of Alkylidene Norcamphors via a Ligand-Controlled Umpolung-Type 1,3-Dipolar Cycloaddition. *iScience* **2019**, *11*, 146 159. (c) Wang, M.; Wang, C.-J.; Lin, Z. Cu(I)/TF-BiphamPhos Catalyzed Reactions of Alkylidene Bisphosphates and Alkylidene Malonates with Azomethine Ylides: Michael Addition versus 1,3-Dipolar Cycloaddition. *Organometallics* **2012**, *31*, 7870 7876. (d) Cabrera, S.; Gómez-Arrayás, R.; Martín-Matute, B.; Cossío, F. P.; Carretero, J. C. Cu^{I} Fesulphos Complexes: Efficient Chiral Catalysts for Asymmetric 1,3-Dipolar Cycloaddition of Azomethine Ylides. *Tetrahedron* **2007**, *63*, 6587. (e) He, Z.-L.; Sheong, F. K.; Li, Q.-H.; Lin, Z.; Wang, C.-J. Exoselective 1,3-Dipolar [3 + 6] Cycloaddition of Azomethine Ylides with 2-Acylcycloheptatrienes: Stereoselectivity and Mechanistic Insight. *Org. Lett.* **2015**, *17*, 1365 1368.

(51) Trost, B. M.; Van Vranken, D. L. Asymmetric Transition Metal-Catalyzed Allylic Alkylations. *Chem. Rev.* **1996**, *96*, 395 422.

(52) (a) Corradini, P.; Maglio, G.; Musco, A.; Paiaro, G. Molecular Asymmetry in π-Allylic Complexes of Transition Metals. *Chem. Commun.* **1966**, *0*, 618 619. (b) Meyer, H.; Zschunke, A. Intramolecular Mobility of η^3-Allylpalladium Chloride Complexes of Different Phosphines Studied by two Dimensional NMR Spectroscopy. *J. Organomet. Chem.* **1984**, *269*, 209. (c) Ogasawara, M.; Takizawa, K.-i.; Hayashi, T. Effects of Bidentate Phosphine Ligands on *syn anti* Isomerization in π-Allylpalladium Complexes. *Organometallics* **2002**, *21*, 4853 4861.

(53) Solin, N.; Szabó, K. J. Mechanism of the η^3 η^1 η^3 Isomerization in Allylpalladium Complexes: Solvent Coordination, Ligand, and Substituent Effects. *Organometallics* **2001**, *20*, 5464 5471.

(54) (a) Collman, J. P.; Hegedus, L. S. *Principles and Applications of Organotransition Metal Chemistry*; University Science Books: Mill Valley, CA, 1980; p 692. (b) Takahashi, T.; Jinbo, Y.; Kitamura, K.; Tsuji, J. Chirality Transfer from C-O to C-C in the Palladium Catalyzed ScN′ Reaction of I- and (Z)-Allylic Carbonates with Carbonucleophile. *Tetrahedron Lett.* **1984**, *25*, 5921 5924. (c) Mackenzie, P. B.; Whelan, J.; Bosnich, B. Asymmetric Synthesis. Mechanism of Asymmetric Catalytic Allylation. *J. Am. Chem. Soc.* **1985**, *107*, 2046 2054. (d) Granberg, K. L.; Baeckvall, J. E. Isomerization of (π-Allyl)Palladium Complexes *via* Nucleophilic Displacement by Palladium(0). A Common Mechanism in Palladium(0)-Catalyzed Allylic Substitution. *J. Am. Chem. Soc.* **1992**, *114*, 6858 6863.

(55) Madrahimov, S. T.; Hartwig, J. F. Origins of Enantioselectivity during Allylic Substitution Reactions. *J. Am. Chem. Soc.* **2012**, *134*, 8136 8147.

(56) (a) Kagan, H. B. Various Aspects of the Reaction of a Chiral Catalyst or Reagent with a Racemic or Enantiopure Substrate. *Tetrahedron* **2001**, *57*, 2449 2468. (b) For a related review, see: Bhat, V.; Welin, E. R.; Guo, X.; Stoltz, B. M. Advances in Stereoconvergent Catalysis from 2005 to 2015: Transition-Metal-Mediated Stereoablative Reactions, Dynamic Kinetic Resolutions, and Dynamic Kinetic Asymmetric Transformations. *Chem. Rev.* **2017**, *117*, 4528 4561.

(57) Arrastia, I.; Arrieta, A.; Cossío, F. P. Application of 1,3-Dipolar Reactions between Azomethine Ylides and Alkenes to the Synthesis of Catalysts and Biologically Active Compounds. *Eur. J. Org. Chem.* **2018**, *2018*, 5889 5904.

(58) (a) Conde, E.; Bello, D.; de Cózar, A.; Sánchez, M.; Vázquez, M. A.; Cossío, F. P. Densely Substituted Unnatural L- and D-prolines as Catalysts for Highly Enantioselective Stereodivergent (3 + 2) Cycloadditions and Aldol Reactions. *Chem. Sci.* **2012**, *3*, 1486 1491. (b) Conde, E.; Rivilla, I.; Larumbe, A.; Cossío, F. P. Enantiodivergent Synthesis of Bis-Spiropyrrolidines via Sequential Interrupted and Completed (3 + 2) Cycloadditions. *J. Org. Chem.* **2015**, *80*, 11755 11767. (c) Pascual-Escudero, A.; de Cózar, A.; Cossío, F. P.; Adrio, J.; Carretero, J. C. Alkenyl Arenes as Dipolarophiles in Catalytic Asymmetric 1,3-Dipolar Cycloaddition Reactions of Azomethine Ylides. *Angew. Chem. Int. Ed.* **2016**, *128*, 15560 15564. (d) Caleffi, G. S.; Larrañaga, O.; Ferrándiz-Saperas, M.; Costa, P. R. R.; Nájera, C.; de Cózar, A.; Cossío, F. P.; Sansano, J. M. Switching Diastereoselectivity in Catalytic Enantioselective (3 + 2) Cycloadditions of Azomethine Ylides Promoted by Metal Salts and Privileged Segphos-Derived Ligands. *J. Org. Chem.* **2019**, *84*, 10593 10605.

(59) Ligands that are large but to some extent flat (instead of isotropically bulky) were shown to build up relatively strong dispersion interactions; see: Wolters, L. P.; Koekkoek, R.; Bickelhaupt, F. M. Role of Steric Attraction and Bite-Angle Flexibility in Metal-Mediated C H Bond Activation. *ACS Catal.* **2015**, *5*, 5766 5775.

(60) Bickelhaupt, F. M.; Houk, K. N. Analyzing Reaction Rates with the Distortion/Interaction-Activation Strain Model. *Angew. Chem. Int. Ed.* **2017**, *56*, 10070 10086.

(61) For selected applications of D/I analysis to organometallic selectivities, see: (a) Green, A. G.; Liu, P.; Merlic, C. A.; Houk, K. N.

https://doi.org/10.1021/jacs.1c12664
J. Am. Chem. Soc. 2022 144 1971 1985

Distortion/Interaction Analysis Reveals the Origins of Selectivities in Iridium-Catalyzed C H Borylation of Substituted Arenes and 5-Membered Heterocycles. *J. Am. Chem. Soc.* **2014**, *136*, 4575 4583. (b) Schoenebeck, F.; Houk, K. N. Ligand-Controlled Regioselectivity in Palladium-Catalyzed Cross Coupling Reactions. *J. Am. Chem. Soc.* **2010**, *132*, 2496 2497. (c) Yu, J.-L.; Zhang, S.-Q.; Hong, X. Mechanisms and Origins of Chemo- and Regioselectivities of Ru(II)-Catalyzed Decarboxylative C H Alkenylation of Aryl Carboxylic Acids with Alkynes: A Computational Study. *J. Am. Chem. Soc.* **2017**, *139*, 7224 7243. (d) Lu, G.; Liu, R. Y.; Yang, Y.; Fang, C.; Lambrecht, D. S.; Buchwald, S. L.; Liu, P. Ligand Substrate Dispersion Facilitates the Copper-Catalyzed Hydroamination of Unactivated Olefins. *J. Am. Chem. Soc.* **2017**, *139*, 16548 16555.

(62) (a) Grimme, S. Do Special Noncovalent π π Stacking Interactions Really Exist? *Angew. Chem. Int. Ed.* **2008**, *47*, 3430 3434. (b) Neel, A. J.; Hilton, M. J.; Sigman, M. S.; Toste, F. D. Exploiting Non-Covalent π Interactions for Catalyst Design. *Nature* **2017**, *543*, 637 646.

(63) Selected related reviews: (a) Trost, B. M.; Crawley, M. L. Asymmetric Transition-Metal-Catalyzed Allylic Alkylations: Applications in Total Synthesis. *Chem. Rev.* **2003**, *103*, 2921 2943. (b) Trost, B. M. Pd Asymmetric Allylic Alkylation (AAA). A Powerful Synthetic Tool. *Chem. Pharm. Bull.* **2002**, *50*, 1 14. (c) Fernandes, R. A.; Nallasivam, J. L. Catalytic Allylic Functionalization *via* π-Allyl Palladium Chemistry. *Org. Biomol. Chem.* **2019**, *17*, 8647 8672.

(64) Trost, B. M.; Hung, M.-H. On the Regiochemistry of Metal-Catalyzed Allylic Alkylation: A Model. *J. Am. Chem. Soc.* **1984**, *106*, 6837 6839.

(65) Selected studies concerning regioselectivities of Pd-catalyzed allylations: (a) Kazmaier, U.; Stolz, D.; Krämer, K.; Zumpe, F. L. Influences on the Regioselectivity of Palladium-Catalyzed Allylic Alkylations. *Chem. Eur. J.* **2008**, *14*, 1322 1329. (b) Hayashi, T.; Kawatsura, M.; Uozumi, Y. Regio- and Enantio-Selective Allylic Alkylation Catalysed by a Chiral Monophosphine Palladium Complex. *Chem. Commun.* **1997**, 561 562. (c) Prétôt, R.; Pfaltz, A. New Ligands for Regio- and Enantiocontrol in Pd-Catalyzed Allylic Alkylations. *Angew. Chem. Int. Ed.* **1998**, *37*, 323 325. (d) Liu, Y.; Jiao, Y.; Luo, H.; Huang, N.; Lai, M.; Zou, K.; Yao, H. Catalyst-Controlled Regiodivergent Synthesis of 1- and 3-Thiosugars with High Stereoselectivity and Chemoselectivity. *ACS Catal.* **2021**, *11*, 5287 5293. (e) Hu, L.; Cai, A.; Wu, Z.; Kleij, A. W.; Huang, G. A Mechanistic Analysis of the Palladium-Catalyzed Formation of Branched Allylic Amines Reveals the Origin of the Regio- and Enantioselectivity through a Unique Inner-Sphere Pathway. *Angew. Chem. Int. Ed.* **2019**, *58*, 14694 14702. (f) Bai, D.-C.; Yu, F.-L.; Wang, W.-Y.; Chen, D.; Li, H.; Liu, Q.-R.; Ding, C.-H.; Chen, B.; Hou, X.-L. Palladium/N-Heterocyclic Carbene Catalysed Regio- and Diastereoselective Reaction of Ketones with Allyl Reagents *via* Inner-Sphere Mechanism. *Nat. Commun.* **2016**, *7*, 11806. (g) Cai, A.; Guo, W.; Martínez-Rodríguez, L.; Kleij, A. W. Palladium-Catalyzed Regio- and Enantioselective Synthesis of Allylic Amines Featuring Tetrasubstituted Tertiary Carbons. *J. Am. Chem. Soc.* **2016**, *138*, 14194 14197. (h) Katcher, M. H.; Sha, A.; Doyle, A. G. Palladium-Catalyzed Regio- and Enantioselective Fluorination of Acyclic Allylic Halides. *J. Am. Chem. Soc.* **2011**, *133*, 15902 15905. (i) Watson, I. D. G.; Yudin, A. K. New Insights into the Mechanism of Palladium-Catalyzed Allylic Amination. *J. Am. Chem. Soc.* **2005**, *127*, 17516 17529.

(66) Madrahimov, S. T.; Li, Q.; Sharma, A.; Hartwig, J. F. Origins of Regioselectivity in Iridium Catalyzed Allylic Substitution. *J. Am. Chem. Soc.* **2015**, *137*, 14968 14981.

(67) (a) Takeuchi, R.; Kashio, M. Highly Selective Allylic Alkylation with a Carbon Nucleophile at the More Substituted Allylic Terminus Catalyzed by an Iridium Complex: An Efficient Method for Constructing Quaternary Carbon Centers. *Angew. Chem. Int. Ed.* **1997**, *36*, 263 265. (b) Janssen, J. P.; Helmchen, G. First Enantioselective Alkylations of Monosubstituted Allylic Acetates Catalyzed by Chiral Iridium Complexes. *Tetrahedron Lett.* **1997**, *38*, 8025 8026.

(68) Selected studies involving regioselectivity of allylation for other metals: (a) Mbaye, M. D.; Demerseman, B.; Renaud, J.-L.; Toupet, L.; Bruneau, C. [Cp (η^2-bipy)(MeCN)Ru^{II}][PF_6] Catalysts for Regioselective Allylic Substitution and Characterization of Dicationic [Cp (η^2-bipy)(η^3-allyl)Ru^{IV}][PF_6]$_2$ Intermediates. *Angew. Chem. Int. Ed.* **2003**, *42*, 5066 5068. (b) Trost, B. M.; Rao, M.; Dieskau, A. P. A Chiral Sulfoxide-Ligated Ruthenium Complex for Asymmetric Catalysis: Enantio- and Regioselective Allylic Substitution. *J. Am. Chem. Soc.* **2013**, *135*, 18697 18704. (c) Ghorai, S.; Chirke, S. S.; Xu, W.-B.; Chen, J.-F.; Li, C. Cobalt-Catalyzed Regio- and Enantioselective Allylic Amination. *J. Am. Chem. Soc.* **2019**, *141*, 11430 11434. (d) Salman, M.; Xu, Y.; Khan, S.; Zhang, J.; Khan, A. Regioselective molybdenum-catalyzed allylic substitution of tertiary allylic electrophiles: methodology development and applications. *Chem. Sci.* **2020**, *11*, 5481 5486. (e) Arnold, J. S.; Mwenda, E. T.; Nguyen, H. M. Rhodium-Catalyzed Sequential Allylic Amination and Olefin Hydroacylation Reactions: Enantioselective Synthesis of Seven-Membered Nitrogen Heterocycles. *Angew. Chem. Int. Ed.* **2014**, *53*, 3688 3692. (f) Arnold, J. S.; Nguyen, H. M. Rhodium-Catalyzed Dynamic Kinetic Asymmetric Transformations of Racemic Tertiary Allylic Trichloroacetimidates with Anilines. *J. Am. Chem. Soc.* **2012**, *134*, 8380 8383. (g) Tang, S.-B.; Zhang, X.; Tu, H.-F.; You, S.-L. Regio- and Enantioselective Rhodium-Catalyzed Allylic Alkylation of Racemic Allylic Alcohols with 1,3-Diketones. *J. Am. Chem. Soc.* **2018**, *140*, 7737 7742.

(69) Hartwig, J. F.; Stanley, L. M. Mechanistically Driven Development of Iridium Catalysts for Asymmetric Allylic Substitution. *Acc. Chem. Res.* **2010**, *43*, 1461 1475.

(70) For selected reviews on Ir-catalyzed allylic substitutions, see: (a) Hartwig, J. F.; Pouy, M. J. Iridium-Catalyzed Allylic Substitution. *Top. Organomet. Chem.* **2011**, *34*, 169 208. (b) Cheng, Q.; Tu, H.-F.; Zheng, C.; Qu, J.-P.; Helmchen, G.; You, S.-L. Iridium-Catalyzed Asymmetric Allylic Substitution Reactions. *Chem. Rev.* **2019**, *119*, 1855 1969. (c) Tosatti, P.; Nelson, A.; Marsden, S. P. Recent Advances and Applications of Iridium-Catalysed Asymmetric Allylic Substitution. *Org. Biomol. Chem.* **2012**, *10*, 3147 3163. (d) Helmchen, G.; Dahnz, A.; Dübon, P.; Schelwies, M.; Weihofen, R. Iridium-Catalysed Asymmetric Allylic Substitutions. *Chem. Commun.* **2007**, 675 691.

(71) (a) Tissot-Croset, K.; Polet, D.; Alexakis, A. A Highly Effective Phosphoramidite Ligand for Asymmetric Allylic Substitution. *Angew. Chem. Int. Ed.* **2004**, *43*, 2426 2428. (b) Rössler, S. L.; Petrone, D. A.; Carreira, E. M. Iridium-Catalyzed Asymmetric Synthesis of Functionally Rich Molecules Enabled by (Phosphoramidite,Olefin) Ligands. *Acc. Chem. Res.* **2019**, *52*, 2657 2672. (c) Teichert, J. F.; Feringa, B. L. Phosphoramidites: Privileged Ligands in Asymmetric Catalysis. *Angew. Chem. Int. Ed.* **2010**, *49*, 2486 2528.

(72) Kiener, C. A.; Shu, C.; Incarvito, C.; Hartwig, J. F. Identification of an Activated Catalyst in the Iridium-Catalyzed Allylic Amination and Etherification. Increased Rates, Scope, and Selectivity. *J. Am. Chem. Soc.* **2003**, *125*, 14272 14273.

(73) Marković, D.; Hartwig, J. F. Resting State and Kinetic Studies on the Asymmetric Allylic Substitutions Catalyzed by Iridium Phosphoramidite Complexes. *J. Am. Chem. Soc.* **2007**, *129*, 11680 11681.

(74) Madrahimov, S. T.; Markovic, D.; Hartwig, J. F. The Allyl Intermediate in Regioselective and Enantioselective Iridium-Catalyzed Asymmetric Allylic Substitution Reactions. *J. Am. Chem. Soc.* **2009**, *131*, 7228 7229.

(75) Leitner, A.; Shekhar, S.; Pouy, M. J.; Hartwig, J. F. A Simple Iridium Catalyst with a Single Resolved Stereocenter for Enantioselective Allylic Amination. Catalyst Selection from Mechanistic Analysis. *J. Am. Chem. Soc.* **2005**, *127*, 15506 15514.

https://doi.org/10.1021/jacs.1c12664
J. Am. Chem. Soc. 2022 144 1971 1985